# Central insulin action regulates peripheral glucose and fat metabolism in mice

Linda Koch,[1] F. Thomas Wunderlich,[1] Jost Seibler,[2] A. Christine Könner,[1] Brigitte Hampel,[1] Sigrid Irlenbusch,[1] Georg Brabant,[3] C. Ronald Kahn,[4] Frieder Schwenk,[2,5] and Jens C. Brüning[1]

[1]Department of Mouse Genetics and Metabolism, Institute for Genetics, University of Cologne, and Center of Molecular Medicine Cologne, Cologne, Germany. [2]TaconicArtemis GmbH, Cologne, Germany. [3]Department of Endocrinology, Christie Hospital, Manchester, United Kingdom. [4]Joslin Diabetes Center, Harvard Medical School, Boston, Massachusetts, USA. [5]Department of Applied Natural Sciences, University of Applied Science Gelsenkirchen, Recklinghausen, Germany.

**Insulin resistance is a hallmark of type 2 diabetes, and many insights into the functions of insulin have been gained through the study of mice lacking the IR. To gain a better understanding of the role of insulin action in the brain versus peripheral tissues, we created 2 mouse models with inducible IR inactivation, 1 in all tissues including brain ($IR^{\Delta wb}$), and 1 restricted to peripheral tissues ($IR^{\Delta per}$). While downregulation of IR expression resulted in severe hyperinsulinemia in both models, hyperglycemia was more pronounced in $IR^{\Delta wb}$ mice. Both strains displayed a dramatic upregulation of hepatic leptin receptor expression, while only $IR^{\Delta per}$ mice displayed increased hepatic Stat3 phosphorylation and Il6 expression. Despite a similar reduction in IR expression in white adipose tissue (WAT) mass in both models, $IR^{\Delta wb}$ mice had a more pronounced reduction in WAT mass and severe hypoleptinemia. Leptin replacement restored hepatic Stat3 phosphorylation and normalized glucose metabolism in these mice, indicating that alterations in glucose metabolism occur largely as a consequence of lipoathrophy upon body-wide IR deletion. Moreover, chronic intracerebroventricular insulin treatment of control mice increased fat mass, fat cell size, and adipose tissue lipoprotein lipase expression, indicating that CNS insulin action promotes lipogenesis. These studies demonstrate that central insulin action plays an important role in regulating WAT mass and glucose metabolism via hepatic Stat3 activation.**

## Introduction

Resistance to the biological effects of the peptide hormone insulin represents one of the hallmarks during the development of type 2 diabetes (1, 2). Apart from the direct effect of impaired insulin action on the dysregulation of glucose and lipid homeostasis (3), insulin resistance predisposes to obesity, atherosclerosis, and cardiovascular diseases (reviewed in refs. 4–6). Nevertheless, the exact molecular mechanisms leading to insulin resistance in patients suffering from type 2 diabetes are largely unknown, and it remains unclear whether they are restricted to selective tissues or represent a more whole-body phenomenon.

Many insights into the molecular mechanisms of insulin action and its role in individual tissues of the mammalian organism have been gained from the inactivation of the *IR* gene in mice, either in a conventional fashion (7, 8) or by conditional inactivation of the IR in selected murine tissues (9–13). These experiments have yielded unexpected findings with respect to the role of insulin action in classical insulin target tissues such as skeletal muscle, liver, and adipose tissue (9, 11, 12), but also in tissues previously viewed as non–insulin responsive, such as brain, pancreatic β cells, macrophages, and blood vessels (10, 13–15). Nevertheless, analyses of tissue- or cell type–specific IR knockout mice are limited by the lack of IR throughout development. Abnormalities arising from impaired insulin action can therefore be partly compensated for by adaptive processes or arise from developmental defects influencing the differentiation of respective tissues.

To study insulin action and insulin resistance in the pathogenesis of type 2 diabetes in adult mice and to circumvent the problem of compensatory changes in the presence of insulin resistance during development, we opted for a time-controlled approach to gene inactivation. To this end, we created mice with an inducible whole body IR deficiency and an inducible IR knockout restricted to peripheral tissues of adult mice. The comparison of the phenotypes of both models allows the observation of consequences of acutely induced insulin resistance for the first time in adult mice and serves as an excellent model for discerning the effects of peripheral versus whole body insulin resistance in the adult mouse.

Taken together, our findings define CNS insulin action as a pivotal determinant of energy homeostasis and peripheral glucose metabolism in the mouse. In addition, our data support recent findings on the regulation of hepatic *Il6* mRNA by central insulin. Nevertheless, leptin-activated Stat3 phosphorylation in liver may alternatively lead to improved glucose metabolism in mice lacking the IR in all tissues, termed $IR^{\Delta wholebody}$ ($IR^{\Delta wb}$) mice. Intriguingly, the more pronounced lipodystrophy in $IR^{\Delta wb}$ mice points to what we believe to be a novel regulatory function of central IR signaling in control of lipogenesis, which is further substantiated by the ability of intracerebroventricularly applied insulin in C57BL/6 mice to slightly increase adipocyte size, fat mass, and white adipose tissue (WAT) lipoprotein lipase expression.

## Results

*Inducible inactivation of the IR gene in peripheral tissues of adult mice.* Mice homozygous for the loxP-flanked IR allele ($IR^{flox/flox}$) were crossed with mice expressing a Cre recombinase fused to the mutated ligand binding domain of the estrogen receptor (ER) from the ubiquitous Rosa26 locus ($Rosa26CreER^{T2}$ mice) (Figure 1A) (16, 17). Upon binding of the synthetic ER antagonist tamoxifen

**Nonstandard abbreviations used:** ER, estrogen receptor; flox, loxP-flanked; ObRb, long isoform of the leptin receptor; WAT, white adipose tissue.

**Conflict of interest:** J. Seibler and F. Schwenk are employees of TaconicArtemis GmbH. All other authors declare that no conflict of interest exists.

**Citation for this article:** *J. Clin. Invest.* **118**:2132–2147 (2008). doi:10.1172/JCI31073.

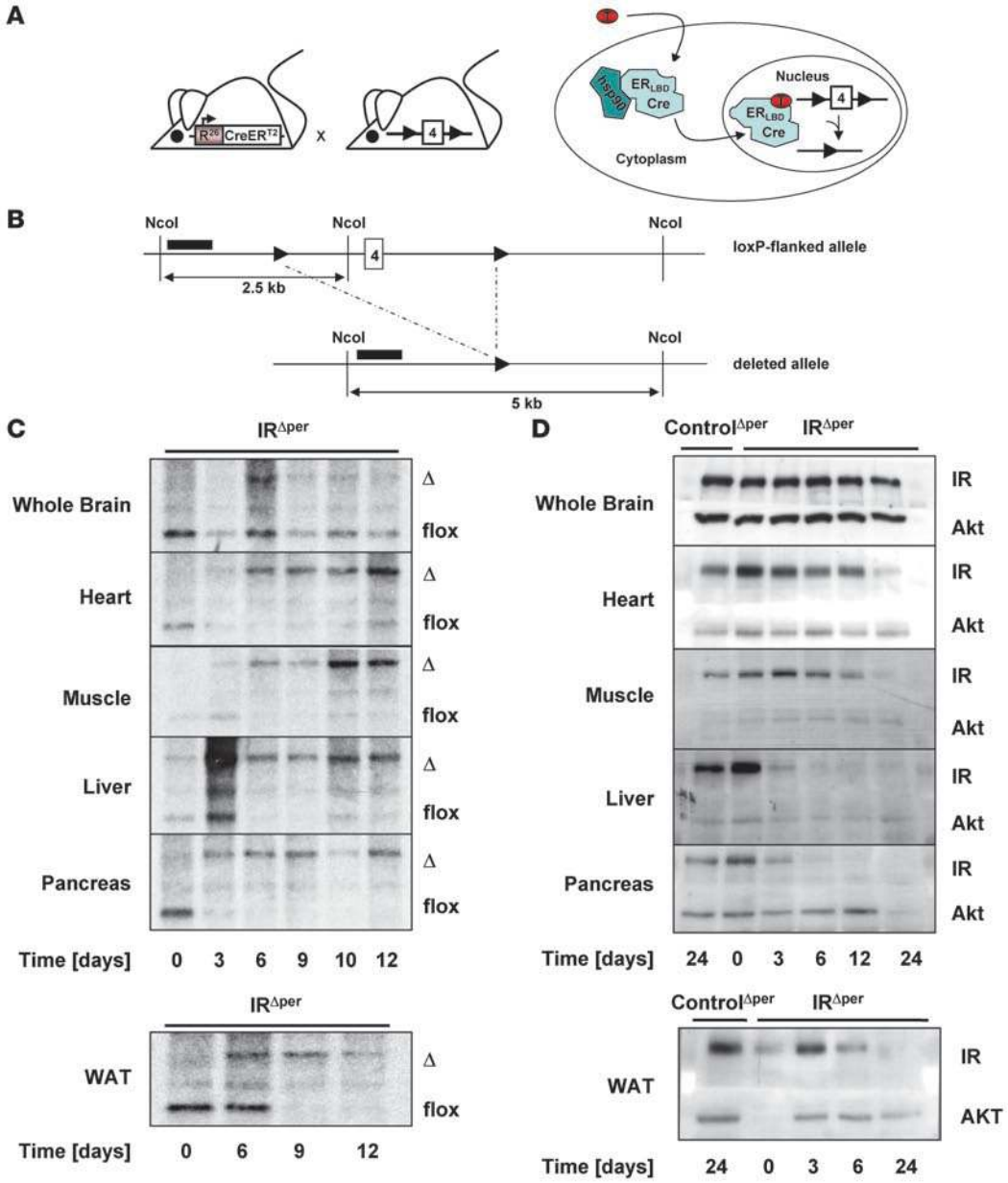


**Figure 1**

Generation of IR$^{\Delta per}$ mice. (**A**) General scheme of the inducible peripheral IR knockout mouse strain. Mice expressing a CreER$^{T2}$ fusion protein under the control of the Rosa26 promoter were crossed with mice homozygous for the floxed IR allele. Binding of tamoxifen (T) to the mutated ligand binding domain of the ER (ER$_{LBD}$) promotes a nuclear import of the fusion protein and results in the excision of exon 4 by the Cre recombinase. (**B**) Genomic map of the mouse IR locus surrounding exon 4. Location of the probe used for Southern blot analysis is indicated by black bars. NcoI, restriction enzyme sites; 4, exon 4 of the *IR* gene; 2.5 kb, size of floxed allele band; 5 kb, size of deleted allele band. (**C**) Southern blot analysis of IR deletion in whole brain, heart, skeletal muscle, liver, pancreas, and WAT of 12-week-old IR$^{\Delta per}$ mice over a period of 12 days. Day 1, beginning of tamoxifen treatment; Δ, 5-kb band of the deleted allele; flox, 2.5-kb band of the floxed allele. (**D**) Western blot analysis of IR and AKT (loading control) in whole brain, heart, skeletal muscle, liver, pancreas, and WAT of tamoxifen-treated 13-week-old IR$^{\Delta per}$ mice and control mice over a period of 24 days. Day 1, beginning of tamoxifen feeding.

to the ER ligand binding domain, the cytoplasmic fusion protein undergoes a conformational change that induces detachment of all heat shock proteins and results in the nuclear import of the fusion protein. In the nucleus, the Cre recombinase mediates the deletion of all floxed alleles (Figure 1A). As previously described for the *RosaCreER*$^{+/-}$ mice (18), recombination occurs with high efficiency only in peripheral tissues, presumably due to a lower local concentration of tamoxifen in the brain.

To inactivate the *IR* gene in peripheral tissues of adult mice in an inducible manner and to control for the metabolic effects of tamoxifen treatment, IR$^{flox/flox}$ mice expressing the Rosa26CreER$^{T2}$ transgene, hereafter termed IR$^{\Delta peripheral}$ (IR$^{\Delta per}$) mice,

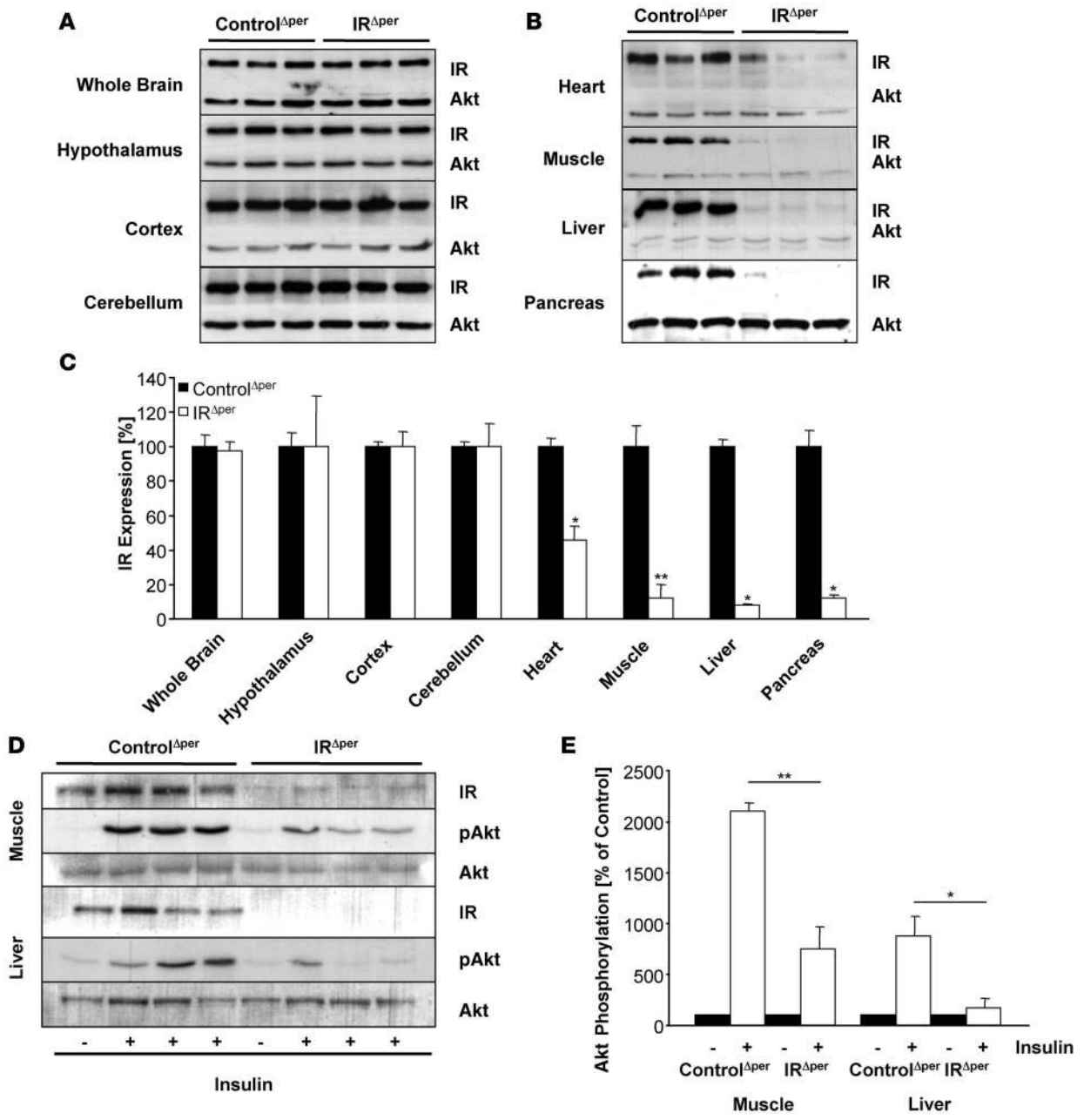


**Figure 2**

IR expression and insulin-stimulated signaling in IR$^{\Delta per}$ mice. (**A**) Western blot analysis of IR and AKT (loading control) in whole brain, hypothalamus, cortex, cerebellum, heart, skeletal muscle, liver, and pancreas of 14-week-old tamoxifen-treated IR$^{\Delta per}$ and Control$^{\Delta per}$ mice. Indicated tissues were dissected 25 days after the last administration of tamoxifen. Animal groups comprised a minimum of 7 IR$^{\Delta per}$ and 9 Control$^{\Delta per}$ mice, except for the western blot analysis in heart, which represents 5 IR$^{\Delta per}$ and 4 Control$^{\Delta per}$ mice. (**B**) Comparative densitometric analysis of IR expression of 14-week-old Control$^{\Delta per}$ (black bars) and IR$^{\Delta per}$ mice (white bars) of the western blot analysis shown in **A**. Values are mean ± SEM. $^{*}P \leq 0.05$; $^{**}P \leq 0.01$ versus control. (**C**) Western blot analysis of IR, pAKT, and AKT (loading control) in skeletal muscle and liver of 14-week-old Control$^{\Delta per}$ and IR$^{\Delta per}$ mice injected with either saline (–) or insulin (+) into the vena cava inferior to assess remaining insulin signaling after IR deletion. Animal groups included 8 IR$^{\Delta per}$ and 8 Control$^{\Delta per}$ mice. (**D**) Comparative densitometric analysis of pAKT of 14-week-old Control$^{\Delta per}$ and IR$^{\Delta per}$ mice of the western blot analysis shown in **C**. pAKT protein amount was normalized to AKT protein expression. pAKT of saline-injected mice was set to 100%. Values are mean ± SEM. $^{*}P \leq 0.05$, $^{**}P \leq 0.01$ versus control. Black bars, saline; white bars, insulin.

and IR$^{flox/flox}$Rosa26CreER$^{T2}$-negative (Control$^{\Delta per}$) mice were treated daily by oral administrations of 5 mg tamoxifen on 5 consecutive days. At various time points during and after the feeding period, tissues were removed from the animals and recombination of the floxed *IR* gene was assessed by Southern blot analysis (Figure 1, B and C). Only 2 days after the start of tamoxifen administration, partial recombination of the floxed *IR* gene was detectable in heart, skeletal muscle, liver, pancreas, and WAT. Recombination

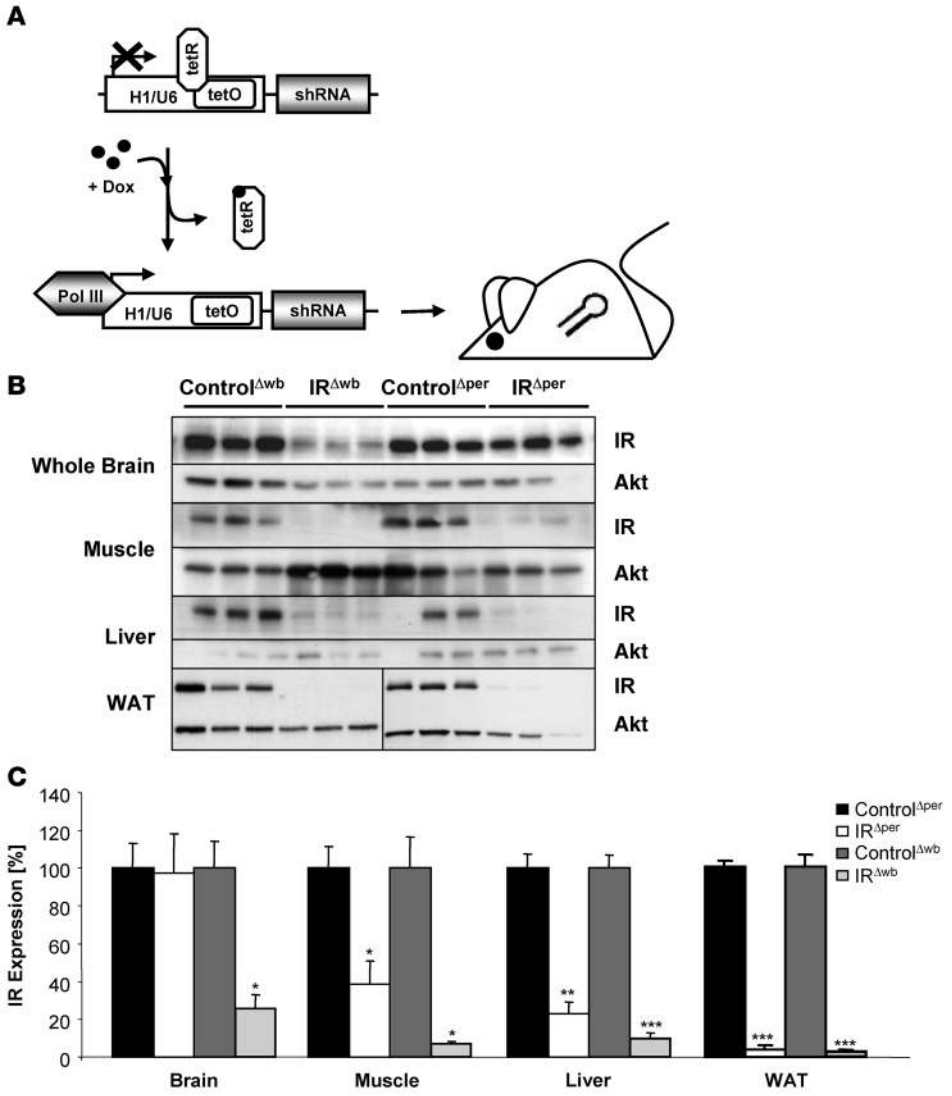


**Figure 3**
Generation of IR$^{\Delta wb}$ mice. (**A**) General scheme of the inducible whole body IR knockout mouse strain. Expression of an IR-specific shRNA is dependent on the RNA-polymerase III–dependent (Pol III–dependent) promoters H1/U6 containing the operator sequences (tetOs) of the *E. coli* tetracycline resistance operon. Binding of the tetracycline repressor (tetR) to tetO prevents transcription. Doxycycline (Dox) sequesters tetR and enables the binding of polymerase III to the H1/U6 promoter, which results in transcription of the shRNA. Binding of the shRNA to complementary mRNAs results in the degradation of the IR mRNA. (**B**) Western blot analysis of IR and AKT (loading control) in whole brain, skeletal muscle, liver, and WAT of 11- to 15-week-old Control$^{\Delta wb}$, IR$^{\Delta wb}$, Control$^{\Delta per}$, and IR$^{\Delta per}$ mice. Tissues were dissected 30 days after the start of inducer administration, except for WAT of Control$^{\Delta wb}$ and IR$^{\Delta wb}$ mice, which was extracted 7 days after start of doxycycline administration. Animal groups were comprised of 3-4 IR$^{\Delta wb}$, 3–4 Control$^{\Delta wb}$, 7–15 IR$^{\Delta per}$, and 9–17 Control$^{\Delta per}$ mice. (**C**) Comparative densitometric analysis of IR expression of 11- to 15-week-old Control$^{\Delta per}$ (black bars), IR$^{\Delta per}$ mice (white bars), Control$^{\Delta wb}$ (dark gray bars), and IR$^{\Delta wb}$ mice (light gray bars) of the western blot analysis shown in **B**. Values are mean ± SEM. $^{*}P \leq 0.05$; $^{**}P \leq 0.01$; $^{***}P \leq 0.001$ versus control. ANOVA values: brain, 0.027; muscle, 0.004; liver, 0.000; WAT, 0.000.

was almost complete on the first day after the last feeding (day 6) (Figure 1C). While deletion was variable in heart, ranging between 70% and 80%, more than 90% of the recombined IR$^{flox/flox}$ allele was detectable in skeletal muscle and liver. The most efficient recombination occurred in pancreas and WAT (Figure 1C), while as expected, less than 15% of the IR$^{flox/flox}$ allele recombined in the CNS.

Taken together, there was efficient tamoxifen-induced recombination of the IR$^{flox/flox}$ allele in IR$^{\Delta per}$ mice in metabolically relevant peripheral tissues such as heart, skeletal muscle, liver, pancreas, and WAT, without significant recombination occurring in the CNS.

To investigate the impact of Cre-mediated recombination on IR protein expression, we performed western blot analyses on tissue lysates obtained from IR$^{\Delta per}$ mice during and after tamoxifen treatment. As expected, the level of immunoreactive IR protein paralleled that of IR$^{flox/flox}$ recombination (Figure 1D). Hence, while there was a decline of IR expression in heart and skeletal muscle over the course of 24 days after the beginning of tamoxifen administration, the maximum reduction of IR expression observed on day 30 was approximately 50% in the former and approximately 90% in the latter, consistent with the presence of unrecombined IR$^{flox/flox}$ alleles in these tissues (Figure 1, C and D, and Figure 2, A and B). Similarly, IR protein expression was virtually abolished in liver, pancreas, and WAT of IR$^{\Delta per}$ mice after completion of tamoxifen treatment (Figure 1D, Figure 2, A and B, and Figure 3A). Protein extracts prepared from whole brain revealed no alteration in immunodetectable IR protein (Figure 1D and Figure 2, A and B). To rule out the possibility that the modest amount of Cre-mediated recombination detectable in whole brain extracts of IR$^{\Delta per}$ mice (Figure 1C) was due to complete recombination in a restricted area of the brain rather than a general low degree of recombination, individual brain regions were probed for immunodetectable IR protein. This analysis revealed unaltered IR expression in hypothalamus, cortex, and cerebellum of tamoxifen-treated IR$^{\Delta per}$ mice (Figure 2, A and B). Hence, consistent with the pattern of DNA recombination, IR protein expression was efficiently reduced in peripheral tissues of IR$^{\Delta per}$ mice without significant alterations in the CNS.

Next, we determined the ability of insulin to activate signaling in skeletal muscle and liver of control and IR$^{\Delta per}$ mice. Consistent with abrogated insulin action as a consequence of IR deficiency, insulin failed to activate phosphorylation of protein kinase B (also known as Akt) at serine residue 473 in skeletal muscle of IR$^{\Delta per}$ mice (Figure 2, C and D). Similarly, insulin-stimulated Akt

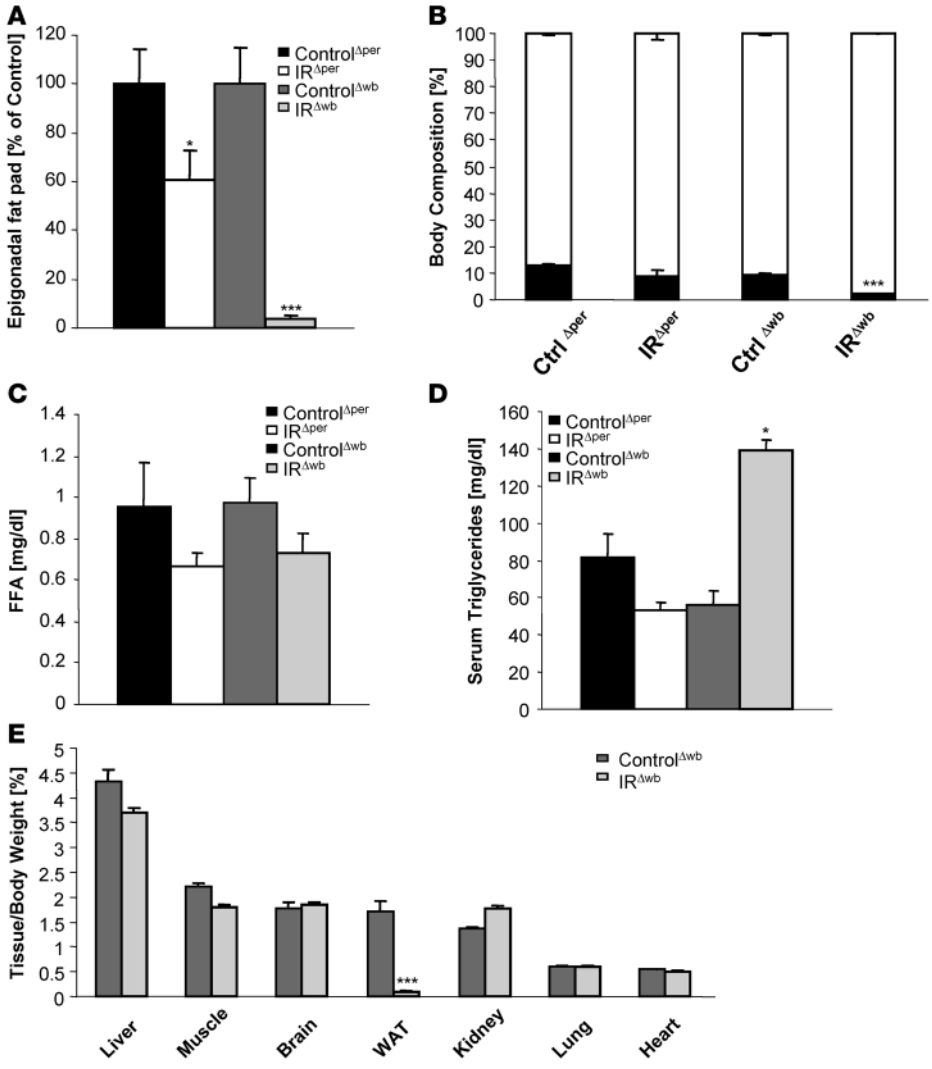


**Figure 4**
Central insulin resistance leads to a more severe lipodystrophy compared with peripheral insulin resistance. (**A**) Average epigonadal fat pad weight of 14-week-old Control$^{\Delta per}$ (black bars, $n$ = 19), IR$^{\Delta per}$ (white bars, $n$ = 18), Control$^{\Delta wb}$ (dark gray bars, $n$ = 18), and IR$^{\Delta wb}$ mice (light gray bars, $n$ = 13) mice 30 days after start of inducer administration. Values are mean ± SEM. $^{*}P \leq 0.05$; $^{***}P \leq 0.001$ versus control. ANOVA value: WAT, 0.000. (**B**) Body composition of 14-week-old Control$^{\Delta per}$ ($n$ = 9), IR$^{\Delta per}$ mice ($n$ = 5), Control$^{\Delta wb}$ ($n$ = 8), and IR$^{\Delta wb}$ mice ($n$ = 12) measured by nuclear magnetic resonance 30 days after start of inducer administration. Black bars indicate fat mass, white bars indicate lean mass. Values are mean ± SEM. $^{***}P \leq 0.001$ versus control. (**C**) Free fatty acids of 14-week-old Control$^{\Delta per}$ (black bars, $n$ = 3), IR$^{\Delta per}$ (white bars, $n$ = 4), Control$^{\Delta wb}$ (dark gray bars, $n$ = 10), and IR$^{\Delta wb}$ mice (light gray bars, $n$ = 11) mice 7 days after start of inducer administration. Values are mean ± SEM. (**D**) Serum triglycerides of 14-week-old Control$^{\Delta per}$ (black bars, $n$ = 5), IR$^{\Delta per}$ (white bars, $n$ = 7), Control$^{\Delta wb}$ (dark gray bars, $n$ = 5), and IR$^{\Delta wb}$ mice (light gray bars, $n$ = 7) mice 7 days after start of inducer administration. Values are mean ± SEM. $^{*}P \leq 0.05$ versus control. (**E**) Tissue weight of liver, muscle, brain, WAT, kidney, lung, and heart correlated with body weight of 14-week-old Control$^{\Delta wb}$ ($n$ = 8–13) and IR$^{\Delta wb}$ mice ($n$ = 8–16) 30 days after start of doxycycline administration. Values are mean ± SEM. $^{***}P \leq 0.001$ versus control.

phosphorylation was reduced by approximately 80% in liver of IR$^{\Delta per}$ mice (Figure 2, C and D).

*Inducible inactivation of the IR in peripheral tissues and the brain*. To investigate the relative contribution of insulin resistance in the CNS in an inducible fashion in addition to peripheral insulin resistance, we employed a second mouse model in which transcription of an shRNA is directed against the IR. This shRNA is under transcriptional control of the human H1/U6 promoter, which contains a tetracycline-operated sequence (tetO). In the presence of the tetracycline repressor (tetR), transcription of the shRNA is silenced. Upon doxycycline administration, the tetR is sequestered from the promoter, thus allowing for ubiquitous transcription of the IR shRNA (Figure 3A) (19, 20). Adult mice carrying this transgene (IR$^{\Delta wb}$) and wild-type littermates (Control$^{\Delta wb}$) were given doxycycline-supplemented water for 30 days, and expression of the IR was analyzed in various tissues. Upon doxycycline-mediated induction of shRNA transcription, there was a similar decrease in IR expression in skeletal muscle and liver compared with expression in the IR$^{\Delta per}$ mice, but additionally there was a significant, more than 90% reduction of IR expression in the CNS (Figure 3, B and C). In conclusion, the 2 inducible insulin resistance mouse models described here displayed a similar degree of IR inactivation in peripheral tissues, while the doxycycline-regulated shRNA expression in IR$^{\Delta wb}$ mice also resulted in the significant reduction of IR expression in the CNS. Thus, a comparative analysis of these 2 mouse strains allows insights into the additional effect of neuronal insulin resistance in comparison with peripheral insulin resistance.

*Central insulin resistance leads to more severe lipodystrophy*. When body weight was measured upon IR inactivation in IR$^{\Delta per}$ and IR$^{\Delta wb}$ mice, it became obvious that acute inactivation of the IR in peripheral tissues of adult mice had little effect on the regulation of body weight. We observed only a transient decrease in body weight between days 6 and 18 after tamoxifen treatment of IR$^{\Delta per}$ mice (Supplemental Figure 1A; supplemental material available online with this article; doi:10.1172/JCI31073DS1). In contrast, IR$^{\Delta wb}$ mice exhibited a continuous decrease in body weight upon induction of the IR shRNA (Supplemental Figure 1A). Interestingly, although both mouse models displayed the same degree of IR deficiency in WAT as determined by western blot analysis (Figure 3, B and C), almost no residual WAT was detectable in IR$^{\Delta wb}$ mice 30 days after start of treatment, while IR$^{\Delta per}$ mice merely exhibited a reduction in WAT mass of 40% (Figure 4A). In accordance, assessment of body com-

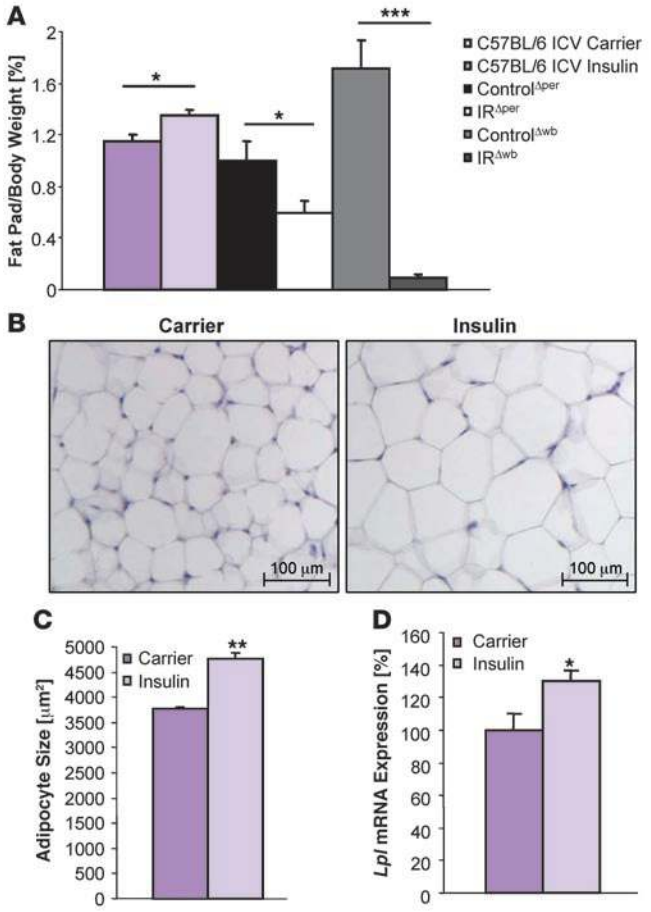


**Figure 5**
Chronic intracerebroventricular infusion of insulin induces lipogenesis in C57BL/6 mice. (**A**) Epigonadal fat pad weight corrected for body weight of 11-week-old C57BL/6 mice receiving chronic intracerebroventricular infusion of carrier (dark purple bars, $n = 5$) or insulin solution (light purple bars, $n = 5$) at a rate of 200 μU/d over 7 days, and of 14-week-old Control$^{\Delta per}$ (black bars, $n = 19$), IR$^{\Delta per}$ (white bars, $n = 15$), Control$^{\Delta wb}$ (dark gray bars, $n = 13$), and IR$^{\Delta wb}$ mice (light gray bars, $n = 16$) mice 30 days after start of inducer administration. Values are mean ± SEM. $^{*}P \leq 0.05$; $^{***}P \leq 0.001$. (**B**) H&E staining of WAT of 11-week-old C57BL/6 mice receiving a chronic intracerebroventricular infusion of carrier or insulin solution at a rate of 200 μU/d over 7 days. Magnification, ×100. (**C**) Mean adipocyte size of 11-week-old C57BL/6 mice receiving chronic intracerebroventricular infusion of carrier (dark purple bar, $n = 3$) or insulin solution (light purple bar, $n = 3$) at a rate of 200 μU/d over 7 days. Values are mean ± SEM. $^{**}P \leq 0.01$ versus control. (**D**) Relative mRNA expression of lipoprotein lipase (LPL) in WAT of 11-week-old C57BL/6 mice receiving chronic intracerebroventricular infusion of carrier (dark purple bar, $n = 5$) or insulin solution (light purple bar, $n = 5$) at a rate of 200 μU/d over 7 days. Values are mean ± SEM. $^{*}P \leq 0.05$ versus control.

position using nuclear magnetic resonance revealed a significant reduction in whole fat mass for IR$^{\Delta wb}$ mice, while the differences in fat mass detected between tamoxifen-treated IR$^{\Delta per}$ mice and littermate controls did not reach significance (Figure 4B). Moreover, while both models of inducible insulin resistance did not result in significantly altered serum concentrations of free fatty acids (Figure 4C), only IR$^{\Delta wb}$ mice exhibited significantly increased plasma triglyceride concentrations (Figure 4D).

To establish whether the reduction in adipose tissue represents a tissue-specific phenomenon or is also detectable in other organs of IR$^{\Delta wb}$ mice, we determined organ weight of liver, skeletal muscle, brain, kidney, lung, and heart of IR$^{\Delta wb}$ mice. This analysis revealed a selectively reduced mass of WAT, while weights of the other organs tested remained unchanged in IR$^{\Delta wb}$ mice compared with controls (Figure 4E). Taken together, these experiments reveal that combined insulin resistance in the CNS and peripheral organs leads to a much more pronounced lipodystrophy than insulin resistance restricted to the periphery, including WAT.

It is well documented that insulin inhibits lipolysis in adipocytes via activation of the IR expressed on these cells (21–23). In light of the more pronounced lipodystrophy detected in IR$^{\Delta wb}$ mice, we next directly addressed whether insulin acting via the CNS has additional effects on adipocyte function. To this end, C57BL/6 mice received a chronic intracerebroventricular infusion of either insulin or carrier solution over a period of 7 days. While insulin administration into the right lateral ventricle did not affect food intake or overall body weight (data not shown), WAT mass of mice receiving intracerebroventricular insulin infusions was slightly but significantly elevated (Figure 5A). The increase in adipose tissue mass was also reflected in an augmented adipocyte size as determined by histological and computational analysis (Figure 5, B and C). In addition, mRNA analysis revealed an increase of the lipogenesis-promoting enzyme lipoprotein lipase in WAT (Figure 5D). These data directly indicate that insulin action in the CNS regions accessible by lateral ventricle insulin infusion, in addition to its fat cell–autonomous inhibition of lipolysis, promotes lipogenesis.

*Insulin inhibits adipocyte-autonomous leptin secretion.* Given the differential regulation of WAT mass, we next measured the concentrations of different adipokines along several time points after induction of IR deficiency in IR$^{\Delta per}$ mice and IR$^{\Delta wb}$ mice. Analysis of circulating serum leptin concentrations showed a constant increase in serum leptin concentrations in IR$^{\Delta per}$ mice compared with control animals after induction of IR deletion in peripheral tissues (Figure 6A). In contrast, deleting the IR additionally in the CNS of IR$^{\Delta wb}$ mice led to a progressive decline in circulating serum leptin concentrations (Figure 6B). However, when leptin concentrations were corrected for epigonadal fat pad weight, both IR$^{\Delta per}$ and IR$^{\Delta wb}$ mice exhibited a staggering increase in leptin levels compared with their tamoxifen- or doxycycline-treated littermate controls (Figure 6C). In a similar manner, while circulating adiponectin concentrations were only decreased in IR$^{\Delta wb}$ mice, serum adiponectin levels were found to be significantly increased in both IR$^{\Delta per}$ and IR$^{\Delta wb}$ mice when correlated with WAT mass (Figure 6, D and E).

In conclusion, lack of IR expression in adipocytes results in an increase in leptin and adiponectin secretion from the adipose tissue. In the case of the IR$^{\Delta wb}$ mice, this effect is masked by the more predominant phenotype of reduced adipose tissue mass, whereas the rise in serum leptin levels remains detectable in the IR$^{\Delta per}$ mice (Figure 6F).

*Peripheral and central insulin action regulate hepatic long isoform of leptin receptor expression.* We next focused on the potential impact of increased leptin concentrations on leptin signal transduction in peripheral tissues by determining the expression of the long isoform of the leptin receptor (ObRb) in liver of IR$^{\Delta per}$ and IR$^{\Delta wb}$ mice. This analysis revealed a striking 76-fold increase in *ObRb* mRNA expression in IR$^{\Delta per}$ compared with control mice (Figure 7A). In IR$^{\Delta wb}$ mice,

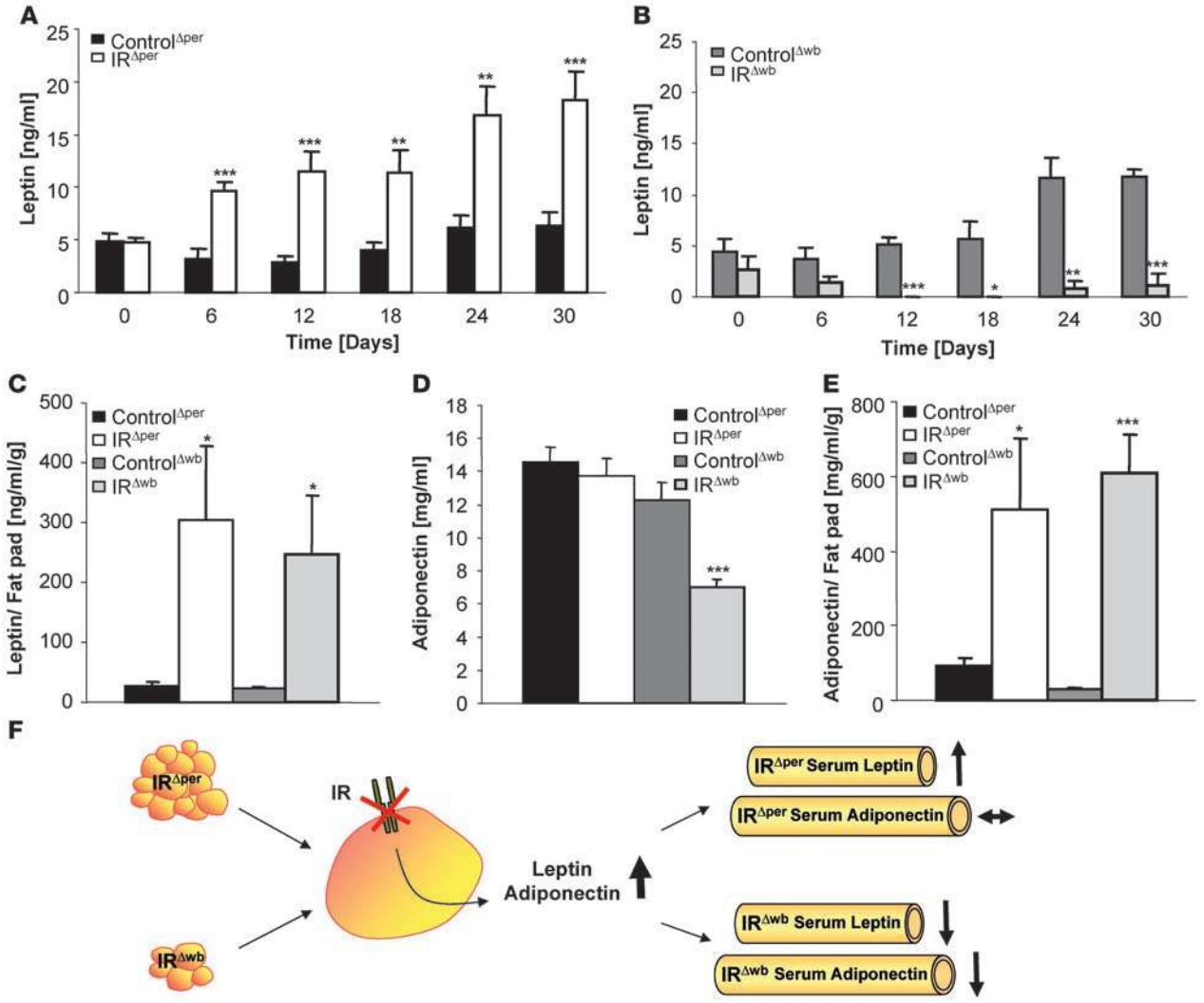


**Figure 6**

Insulin inhibits cell-autonomous leptin secretion. (**A**) Serum leptin levels of 14-week-old Control$^{\Delta per}$ ($n$ = 18) and IR$^{\Delta per}$ mice ($n$ = 18) over a period of 30 days. Values are mean ± SEM. $^{**}P \le 0.01$, $^{***}P \le 0.001$ versus control. (**B**) Serum leptin levels of 14-week-old Control$^{\Delta wb}$ ($n$ = 5) and IR$^{\Delta wb}$ mice ($n$ = 5) over the course of 30 days. Values are mean ± SEM. $^{*}P \le 0.05$, $^{**}P \le 0.01$, $^{***}P \le 0.001$ versus control. (**C**) Serum leptin levels correlated with epigonadal fat pad weight of 14-week-old Control$^{\Delta per}$ (black bar; $n$ = 17), IR$^{\Delta per}$ (white bar; $n$ = 13), Control$^{\Delta wb}$ (dark gray bar; $n$ = 13), and IR$^{\Delta wb}$ mice (light gray bar; $n$ = 6). Concentrations were measured 30 days after start of tamoxifen or doxycycline administration. Values are mean ± SEM. $^{*}P \le 0.05$ versus control. (**D**) Serum adiponectin levels of 14-week-old Control$^{\Delta per}$ (black bar; $n$ = 13), IR$^{\Delta per}$ (white bar; $n$ = 8), Control$^{\Delta wb}$ (dark gray bar; $n$ = 13), and IR$^{\Delta wb}$ mice (light gray bar; $n$ = 18). Samples were taken 30 days after start of tamoxifen or doxycycline administration. Values are mean ± SEM. $^{***}P \le 0.001$ versus control. (**E**) Serum adiponectin levels correlated with epigonadal fat pad weight of 14-week-old Control$^{\Delta per}$ (black bar; $n$ = 13), IR$^{\Delta per}$ (white bar; $n$ = 10), Control$^{\Delta wb}$ (dark gray bar; $n$ = 13), and IR$^{\Delta wb}$ mice (light gray bar; $n$ = 16). Samples were taken 30 days after start of tamoxifen or doxycycline administration. Values are mean ± SEM. $^{*}P \le 0.05$; $^{*}P \le 0.001$ versus control. (**F**) General scheme for the effects of insulin resistance on circulating leptin and adiponectin levels. As a result of the loss of peripheral IR signaling, leptin and adiponectin secretion is disinhibited, resulting in an increase in circulating concentrations, still detectable in the raised leptin levels of IR$^{\Delta per}$ mice. However, in IR$^{\Delta wb}$ mice this effect is masked by a dramatic reduction in WAT mass.

a significant increase in hepatic *ObRb* mRNA expression could also be detected, although to a lesser extent than in IR$^{\Delta per}$ mice (Figure 7B). In both mouse models, the rise in *ObRb* mRNA was reflected by a dramatic increase in ObRb protein expression, as shown by western blot analysis, while almost no immunoreactive ObRb was present in the liver of tamoxifen- or doxycycline-treated control mice (Figure 7C).

To determine whether a rise in hepatic ObRb expression in the presence of elevated leptin concentrations resulted in increased leptin receptor signaling, we next determined the expression and tyrosine phosphorylation of a downstream target of leptin signaling, Stat3. While hepatic Stat3 protein expression remained indistinguishable between control and IR$^{\Delta per}$ mice, a significant increase in tyrosine phosphorylated Stat3 could be detected in IR$^{\Delta per}$ mice (Figure 7D). In contrast, both expression and tyrosine phosphorylation of Stat3 were unaltered in IR$^{\Delta wb}$ mice compared with control mice (Figure 7E). When combined, these findings show that both acute selective peripheral and whole body insulin resistance lead to ObRb upregulation in liver.

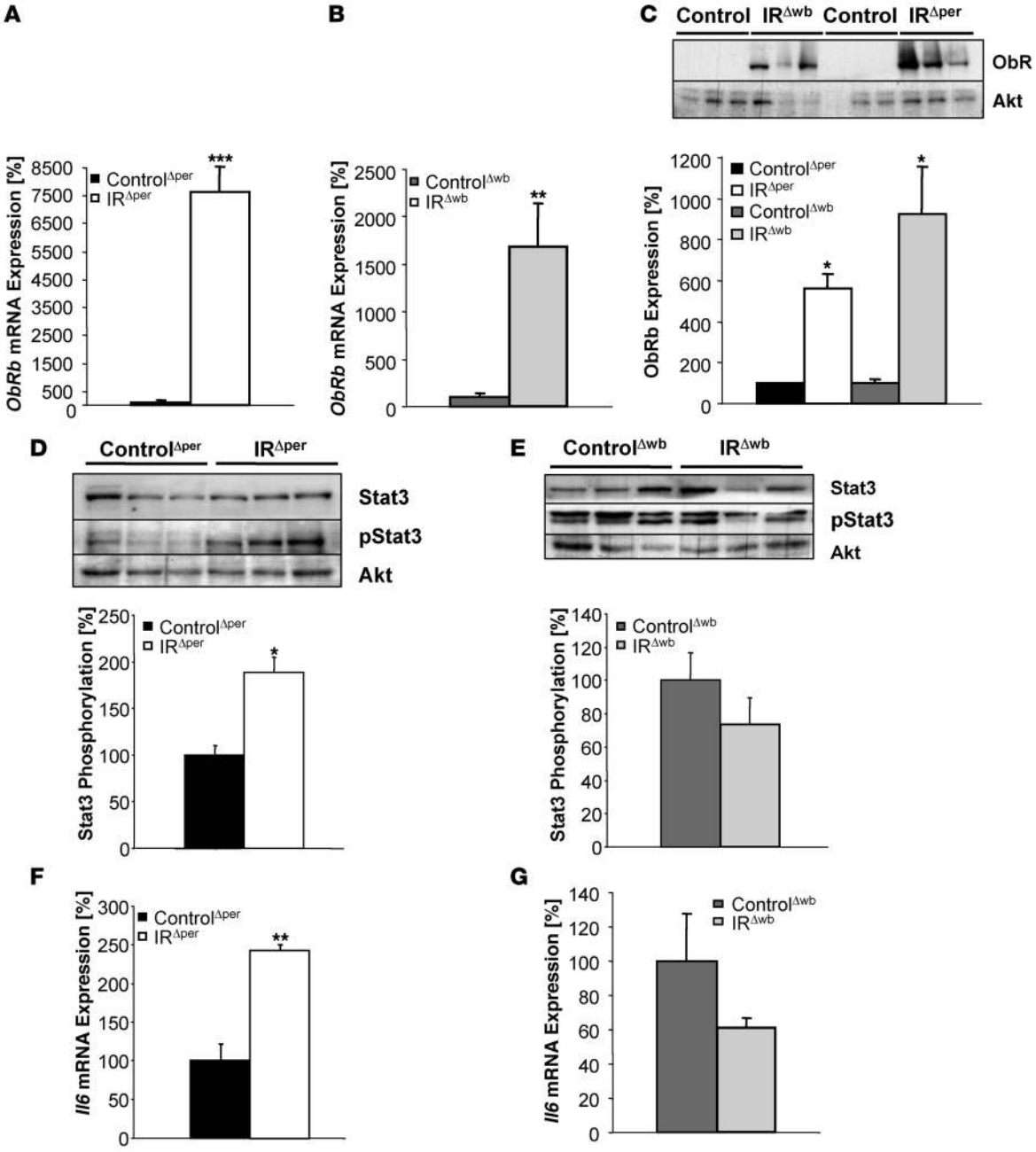


**Figure 7**

Effects of insulin resistance on leptin receptor expression, Stat3 phosphorylation, and *Il6* mRNA expression in liver of 14-week-old $IR^{\Delta per}$ and $IR^{\Delta wb}$ mice. Relative mRNA expression of hepatic *ObRb* of (**A**) $Control^{\Delta per}$ (black bar; $n = 8$) and $IR^{\Delta per}$ (white bar; $n = 7$) mice and (**B**) $Control^{\Delta wb}$ (dark gray bar; $n = 5$) and $IR^{\Delta wb}$ (light gray bar; $n = 4$) mice. (**C**) Western blot and densitometric analysis of hepatic ObRb and Akt (loading control) of $Control^{\Delta wb}$ ($n = 3$), $IR^{\Delta wb}$ ($n = 3$), $Control^{\Delta per}$ ($n = 9$), and $IR^{\Delta per}$ ($n = 9$) mice, with mean ObRb expression of controls set to 100%. (**D**) Western blot and densitometric analysis of hepatic Stat3, phosphorylated Stat3, and AKT of $Control^{\Delta per}$ ($n \geq 6$) and $IR^{\Delta per}$ ($n \geq 6$) mice, with mean phosphorylated Stat3 in $Control^{\Delta per}$ mice set to 100%. (**E**) Western blot and densitometric analysis of hepatic Stat3, phosphorylated Stat3, and Akt of $Control^{\Delta wb}$ and $IR^{\Delta wb}$ mice, with mean phosphorylated Stat3 in $Control^{\Delta wb}$ mice set to 100%. $n \geq 3$ mice per group for Stat3 and $n \geq 7$ mice per group for phosphorylated Stat3 analysis. Relative mRNA expression of hepatic *Il6* in (**F**) $Control^{\Delta per}$ (black bar; $n = 8$) and $IR^{\Delta per}$ (white bar; $n = 7$) mice and (**G**) $Control^{\Delta wb}$ (dark gray bar; $n = 7$) and $IR^{\Delta wb}$ (light gray bar; $n = 7$) mice. Samples were collected 30 days after starting each experiment. Values are mean ± SEM. $^{*}P \leq 0.05$, $^{**}P \leq 0.01$, $^{***}P \leq 0.001$ versus control.

*Central insulin action regulates hepatic Il6 mRNA levels*. Recently, insulin was demonstrated to activate hypothalamic insulin signaling, leading to increased hepatic *Il6* mRNA expression and resulting in Stat3 phosphorylation in hepatocytes (24), a process specifically regulated via Agouti-related peptide neurons (25). Since IR expression in the brain is unaltered in $IR^{\Delta per}$ mice and these mice exhibit increased circulating serum insulin concentrations, we hypothesized that intact neuronal insulin signal transduction may lead to

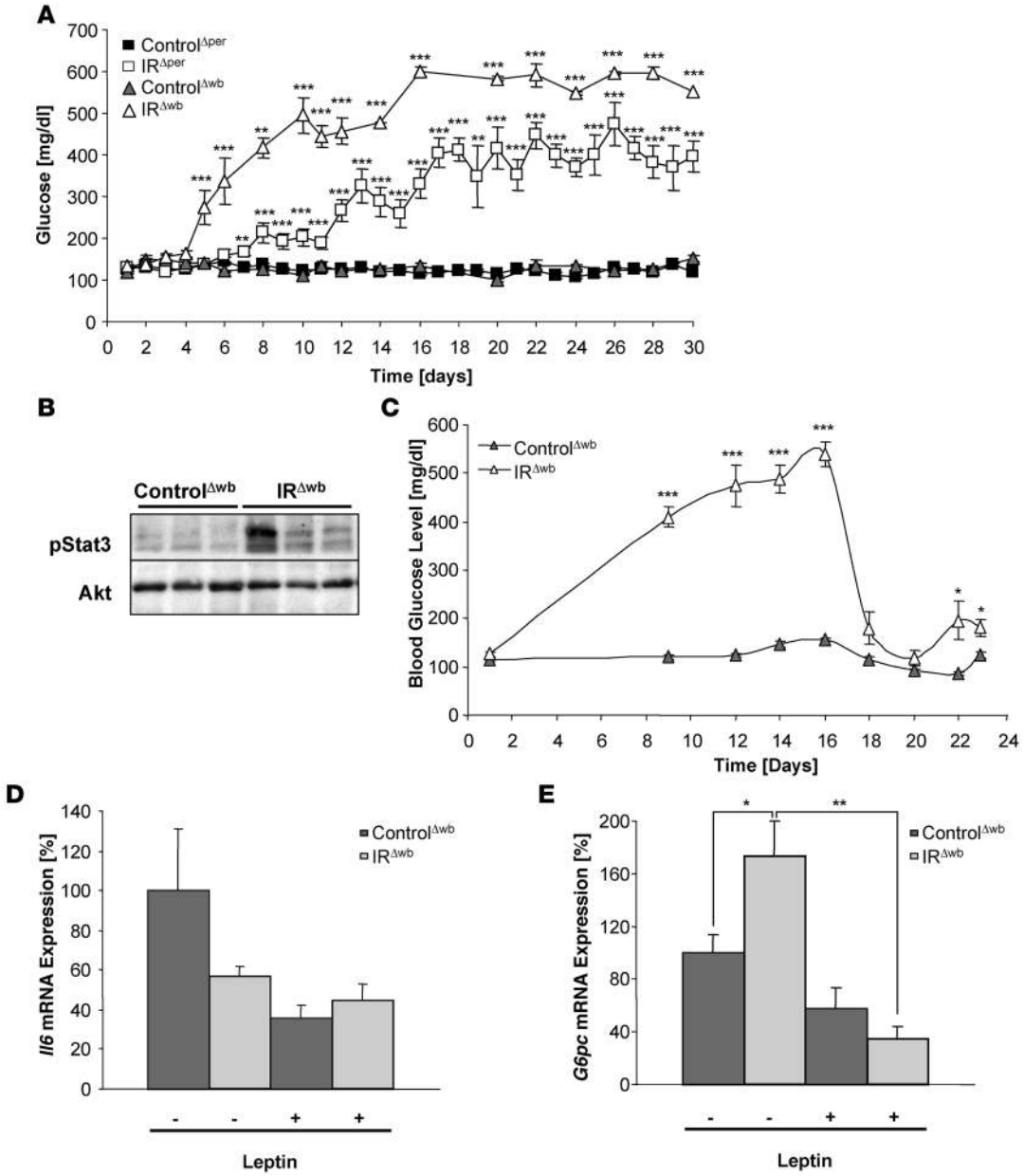


**Figure 8**

Restoration of Stat3 phosphorylation in IR$^{\Delta wb}$ mice ameliorates hyperglycemia. (**A**) Random fed blood glucose concentrations of 14-week-old Control$^{\Delta per}$ (filled squares; $n$ = 3–50), IR$^{\Delta per}$ (open squares; $n$ = 3–48), Control$^{\Delta wb}$ (filled triangles; $n$ = 5–27) and IR$^{\Delta wb}$ mice (open triangles; $n$ = 5–32) over 30 days. Data represent the mean ± SEM. $^{**}P \leq 0.01$, $^{***}P \leq 0.001$ versus control. (**B**) Western blot analysis of phosphorylated Stat3 and AKT (loading control) in liver of 13-week-old Control$^{\Delta wb}$ and IR$^{\Delta wb}$ mice receiving a chronic infusion of leptin at a rate of 12 μg per day. Tissues were excised 7 days after the subcutaneous implantation of an osmotic mini-pump. (**C**) Random fed blood glucose concentrations of 13-week-old Control$^{\Delta wb}$ (filled triangles; $n$ = 5) and IR$^{\Delta wb}$ mice (open triangles; $n$ = 5) receiving a chronic infusion of leptin at a rate of 12 μg per day from day 16 onward. Data represent the mean ± SEM. $^{*}P \leq 0.05$, $^{***}P \leq 0.001$ versus control. (**D**) Relative mRNA expression of *Il6* in liver of 14-week-old Control$^{\Delta wb}$ (dark gray bars; $n$ = 5) and IR$^{\Delta wb}$ (light gray bars; $n$ = 5) mice before (–) and after (+) chronic infusion of leptin at a rate of 12 μg per day over 7 days. Values are means ± SEM. (**E**) Relative mRNA expression of glucose-6-phosphatase (*G6P*) in liver of 14-week-old Control$^{\Delta wb}$ (dark gray bars; $n$ = 5) and IR$^{\Delta wb}$ (light gray bars; $n$ = 5) mice before (–) and after (+) chronic infusion of leptin at a rate of 12 μg per day over 7 days. Values are mean ± SEM. $^{*}P \leq 0.05$, $^{**}P \leq 0.01$ versus control.

upregulation of hepatic *Il6* mRNA expression. Indeed, we observed a significant 2.5-fold upregulation of *Il6* mRNA expression in the liver of IR$^{\Delta per}$ mice (Figure 7F). Thus, the observed increased Stat3 phosphorylation in the liver of IR$^{\Delta per}$ mice may result either from signal transduction via the hepatic ObRb or via the hepatic Il6 receptor, possibly as a consequence of intact neuronal insulin signaling in the presence of elevated serum insulin concentrations. In contrast to that seen in IR$^{\Delta per}$ mice, hepatic *Il6* mRNA expression remained unaltered in IR$^{\Delta wb}$ mice (Figure 7G), supporting a role for central insulin in the regulation of hepatic *Il6* mRNA expression.

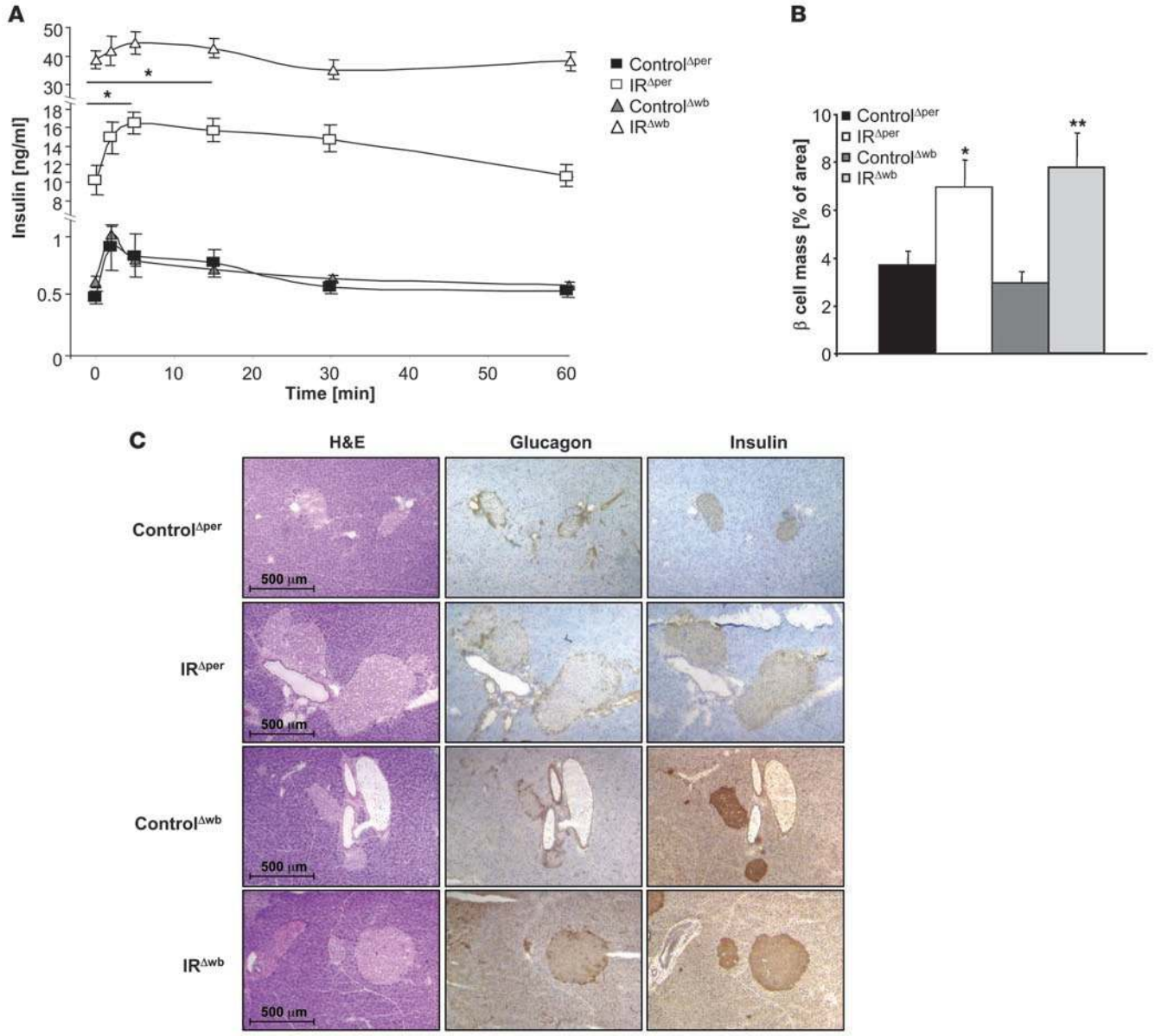


**Figure 9**

Plasma insulin levels and glucose-stimulated insulin secretion in IR$^{\Delta per}$ and IR$^{\Delta wb}$ mice. (**A**) Glucose-stimulated insulin secretion of 13-week-old Control$^{\Delta per}$ (filled squares; $n = 8$), IR$^{\Delta per}$ (open squares; $n = 5$), Control$^{\Delta wb}$ (filled triangles; $n = 5$), and IR$^{\Delta wb}$ mice (open triangles; $n = 8$) on day 18. Values are mean ± SEM. *$P \leq 0.05$ versus 0 min. (**B**) Percentage of β cell mass in 14-week-old Control$^{\Delta per}$ (black bars; $n = 4$), IR$^{\Delta per}$ mice (white bars; $n = 4$), Control$^{\Delta wb}$ (dark gray bars; $n = 3$), and IR$^{\Delta wb}$ mice (light gray bars; $n = 3$). Data was collected 30 days after starting the experiment. Values are mean ± SEM. *$P \leq 0.05$, **$P \leq 0.01$ versus control. (**C**) Immunohistochemical stainings of pancreatic islets in 14-week-old Control$^{\Delta per}$, IR$^{\Delta per}$, Control$^{\Delta wb}$, and IR$^{\Delta wb}$ mice. Pancreatic tissues were stained for H&E, insulin, and glucagon. Magnification, ×100.

*IR$^{\Delta wb}$ mice display a higher degree of impaired peripheral glucose metabolism.* To determine the regulation of peripheral glucose metabolism after acute induction of peripheral or whole body insulin resistance, blood glucose levels in randomly fed mice were assessed daily from the period of induction with either tamoxifen in IR$^{\Delta per}$ or doxycycline in IR$^{\Delta wb}$ mice. An early onset rise of blood glucose concentrations in IR$^{\Delta wb}$ mice was observed, reaching 600 mg/dl 17 days after the beginning of doxycycline induction (Figure 8A). IR$^{\Delta per}$ mice also exhibited a clear increase in blood glucose concentrations after completion of tamoxifen treatment. Nevertheless, both the kinetics of hyperglycemia onset and the magnitude of hyperglycemia reached were significantly lower in IR$^{\Delta per}$ mice (Figure 8A). Blood glucose concentration reached the maximum of approximately 400 mg/dl 17 days after start of tamoxifen administration and stayed stable in this range during the following 2 weeks (Figure 8A). Accordingly, glucose tolerance tests performed at day 18 after induction of IR ablation in both mouse models disclosed a significant impairment of glucose tolerance in IR$^{\Delta per}$ mice (Supplemental Figure 1B). Fasting blood glucose concentrations remained unaltered at the same time point (Supplemental Figure 1B). IR$^{\Delta wb}$ mice, on the other hand,

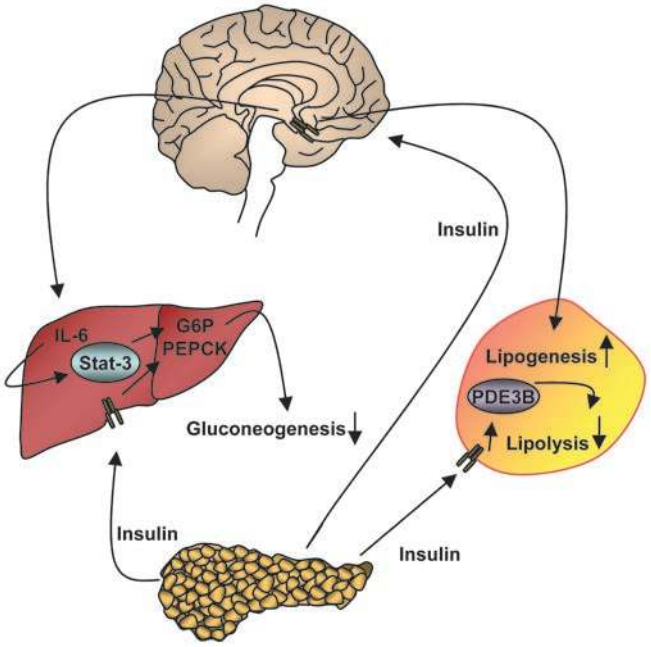


**Figure 10**
Proposed model for insulin action in the CNS and in the periphery in the regulation of glucose and adipose tissue metabolism. Insulin is secreted from the pancreas and binds directly to IRs on peripheral organs such as liver and adipose tissue, thereby mediating signals leading to the downregulation of gluconeogenesis and lipolysis. By binding and activating IRs in the CNS, insulin action ultimately leads to the activation of hepatic Il6 and the upregulation of lipogenic genes in WAT.

exhibited a significant increase in fasting blood glucose concentrations but also reacted with a significant rise in blood glucose concentrations upon exogenous glucose administration (Supplemental Figure 1C). Since IR deletion occurred to a similar extent in peripheral tissues of $IR^{\Delta per}$ and $IR^{\Delta wb}$ mice, these data indicate that lack of the IR in the CNS of $IR^{\Delta wb}$ mice leads to a significantly more severe impairment of peripheral glucose homeostasis.

*Leptin administration improves glucose metabolism in $IR^{\Delta wb}$ mice*. To analyze whether loss of signaling via hepatic Stat3 in $IR^{\Delta wb}$ mice, either as a consequence of reduced hepatic Il6 expression or due to the absence of leptin, contributes to the impairment of peripheral glucose homeostasis, doxycycline-treated $IR^{\Delta wb}$ mice and littermate controls received a chronic leptin infusion over a period of 7 days via subcutaneously implanted osmotic mini-pumps. Serum leptin levels were measured immediately before and at several time points during chronic administration of leptin. Both in $IR^{\Delta wb}$ mice and littermate controls, leptin levels were significantly increased as early as 2 days after pump implant and remained high over the course of the experiment (Supplemental Figure 2A). Western blot analysis revealed the restoration of hepatic Stat3 tyrosine phosphorylation after leptin reconstitution in $IR^{\Delta wb}$ mice, whereas no increase in phosphorylated Stat3 could be detected in controls receiving leptin infusions (Figure 8B), consistent with the very low abundance of ObRb expression in liver of control mice (Figure 7, A–C). Strikingly, in parallel to increased Stat3 phosphorylation in $IR^{\Delta wb}$ mice receiving leptin infusion, blood glucose levels decreased dramatically 2 days after the start of leptin infusion to levels comparable with those found in control mice (Figure 8C). Notably, blood glucose concentrations were completely normalized only for the period of time when leptin replacement achieved plasma leptin concentrations exceeding those observed in $IR^{\Delta per}$ mice. Nevertheless, when plasma leptin concentrations declined over time, reaching concentrations found in $IR^{\Delta per}$ mice, a significant improvement of glucose metabolism could still be observed (Figure 8C and Supplemental Figure 2A). To discern whether leptin restoration improves glucose metabolism in $IR^{\Delta wb}$ mice via direct ObRb-mediated signaling or indirectly via upregulation of hepatic Il6 expression, we next determined hepatic *Il6* mRNA expression in control and $IR^{\Delta wb}$ mice before and during leptin replacement. This analysis revealed that leptin restoration does not upregulate hepatic *Il6* mRNA expression (Figure 8D), supporting the notion that leptin acts directly via hepatic ObRb signaling to activate Stat3 and to restore glucose metabolism in $IR^{\Delta wb}$ mice. In addition, these findings suggest that hepatic *Il6* mRNA expression is controlled by central insulin action. Moreover, leptin restoration in $IR^{\Delta wb}$ mice resulted in a significant reduction of *glucose-6-phosphatase* mRNA expression, which was initially increased in $IR^{\Delta wb}$ mice (Figure 8E). Taken together, these data show that restoring hepatic Stat3 activation largely ameliorates dysregulated glucose metabolism in $IR^{\Delta wb}$ mice, at least in part by repressing hepatic gluconeogenesis.

*Peripheral and central insulin resistance result in β cell hyperplasia*. Because insulin resistance restricted to pancreatic β cells throughout development has been demonstrated to impair insulin secretion, we determined serum insulin concentrations and the insulin secretion response to exogenously applied glucose in $IR^{\Delta per}$ and $IR^{\Delta wb}$ mice. Assessment of serum insulin concentrations revealed a similarly significant degree of hyperinsulinemia as an indirect measure of peripheral insulin resistance in both $IR^{\Delta per}$ and $IR^{\Delta wb}$ mice upon induction of IR ablation (Supplemental Figure 2B). $IR^{\Delta per}$ mice reached a maximum 50-fold increase on day 18, while $IR^{\Delta wb}$ mice displayed their maximum on day 12 following the induction of IR ablation (Supplemental Figure 2B).

Further analysis revealed a significant increase in fasting serum insulin concentrations in $IR^{\Delta per}$ and even higher levels in $IR^{\Delta wb}$ mice, consistent with the degree of insulin resistance in these mouse models (Figure 9A). Following an intravenous injection of glucose, serum insulin concentrations of $IR^{\Delta per}$ mice were significantly elevated, both acutely within 5 minutes after glucose injections and in a prolonged fashion 30 minutes after injection (Figure 9A), whereas this pattern of glucose-stimulated insulin secretion appeared altered in $IR^{\Delta wb}$ mice. However, given the dramatic increase in fasting plasma insulin concentrations in $IR^{\Delta wb}$ mice, it may be difficult to draw conclusions on insulin secretion patterns in this situation.

Histological analysis of pancreatic tissues revealed a clear β cell hyperplasia upon induced IR ablation in both mouse models, consistent with the β cell proliferative response to insulin resistance (Figure 9, B and C). Quantitative assessment of β cell mass revealed a 2-fold increase in β cell mass 3 weeks after induction of IR deficiency, indicating a fast hyperproliferative β cell response to peripheral insulin resistance (Figure 9B). On the other hand, despite a significant enlargement of pancreatic islets both in $IR^{\Delta per}$ and $IR^{\Delta wb}$ mice, their architecture appeared normal, with unaltered distribution of insulin-producing β cells and glucagon-producing α cells (Figure 9C).

These data indicate that in response to acutely induced insulin resistance in adult mice, even within pancreatic β cells themselves, β cell mass remains dynamic and still allows for the occurrence of β cell hyperplasia.

## Discussion

Over the past few years, it has become widely acknowledged that insulin has profound effects in the CNS, where it modulates a variety of functions, including the regulation of food intake, sympathetic activity, peripheral glucose homeostasis, and reproductive endocrinology (10, 26–28). To elucidate the contribution of brain insulin signaling compared with peripheral insulin signaling with respect to the pathophysiology of insulin resistance, we have employed 2 acutely inducible IR-deficient mouse models. The $IR^{\Delta wb}$ mice showed a strong reduction of the IR in all tissues including the CNS, whereas the $IR^{\Delta per}$ mice lacked the IR only in the periphery.

The $IR^{\Delta per}$ mouse model uses a Cre recombinase–steroid receptor fusion protein to acutely induce a peripheral IR knockout. These $RosaCreER^{T2}$-expressing mice showed little or no recombination in brain, thought to be an effect of a lower local concentration of tamoxifen in the CNS (18) potentially attributable to low-efficiency transport of tamoxifen through the blood-brain barrier. Therefore, this model serves as an ideal tool for analyzing the effects of acutely induced peripheral insulin resistance. The $IR^{\Delta wb}$ mouse model employs the method of conditional RNAi-mediated gene knockdown through the expression of an ubiquitous IR-specific shRNA. In both models the onset of systemic insulin resistance can be modulated through administration of inducers, tamoxifen in $IR^{\Delta per}$ mice and doxycycline in $IR^{\Delta wb}$ mice. Our findings show the successful generation of 2 inducible insulin resistance models that serve to study the role of insulin action and insulin resistance devoid of any developmental compensation, thus bypassing any changes arising from deletion of the IR during embryonic development. As type 2 diabetes in humans manifests itself at a later stage in life, the adult mouse model is more likely to yield insights into the consequences of acquired insulin resistance.

Recent studies have provided increasing evidence for a role of neuronal insulin action in the maintenance of glucose homeostasis (26, 29–33). Nevertheless, it remains debated whether insulin's direct or indirect effects on peripheral tissues are more important determinants in these mechanisms. On the one hand, Edgerton et al. have shown that insulin's direct effects on the liver regarding the control of hepatic glucose production prove dominant over indirect effects in conscious dogs (34). The importance of insulin's direct effects has also been elaborately described by the analysis of liver-specific IR knockout mice, which exhibit increased plasma insulin levels and signs of hepatic insulin resistance (12). In contrast, the neuron-specific IR knockout mouse shows moderate signs of diet-dependent obesity but also impaired supression of hepatic glucose production (10), evidence for a significant indirect effect of insulin signaling in the regulation of hepatic glucose production. This is supported by studies employing injections of antisense oligonucleotides to impair IR signaling selectively in the mediobasal hypothalamus (26, 29). These controversial findings have been subject to extensive discussion and, along with other findings, have been attributed to differences of glucose metabolism in different species (35). The present study reveals several aspects we believe to be novel in understanding the consequences, and particularly the relative contribution, of CNS insulin action to metabolic regulation.

Both $IR^{\Delta per}$ and $IR^{\Delta wb}$ mice displayed a significant reduction of WAT mass, which was expected to a certain degree due to the loss of inhibition of lipolysis by insulin, owing to the cell-autonomous action of insulin on adipocytes and consistent with a reduction of fat mass in fat-specific IR knockout mice (9). Surprisingly, the loss of epigonadal fat pads in $IR^{\Delta wb}$ mice was much more pronounced compared with $IR^{\Delta per}$ mice in the presence of the same degree of IR ablation in adipose tissue. Body composition analysis revealed a significantly more pronounced loss of fat mass in $IR^{\Delta wb}$ mice, while the size of other organs remained unaltered. Recent studies suggest the presence of a newly discovered neuroendocrine circuit in the CNS involving ghrelin, which is responsible for the regulation of metabolism in adipose tissue (36). Chronic intracerebroventricular administration of ghrelin resulted in an increase in glucose and triglyceride uptake in white adipocytes, inhibition of lipid oxidation, and a rise in lipogenesis (36). Our findings suggest a role for central insulin in this CNS neuroendocrine network of adipose metabolism. Chronic intracerebroventricular infusion of insulin into the lateral ventricle of C57BL/6 mice resulted in a slightly increased epigonadal fat pad mass, larger adipocytes, and an increase in the fat storage–promoting enzyme lipoprotein lipase compared with mice receiving carrier infusion. As mentioned before, isolated neuronal insulin resistance, either via tissue-specific knockout mouse models (10) or through injection of either antisense oligonucleotides directed against the IR (26, 29) or lentiviral-mediated knockdown of the IR in the mediobasal hypothalamus in rats (37), has been shown to result in a modest increase in fat pad mass and mild obesity. The increase in body weight as a consequence of central insulin resistance appears to result from hyperphagia and/or altered energy expenditure. Nevertheless, the phenotype of NIRKO mice is confounded by hypogonadism in these animals. Lateral intracerebroventricular infusion of insulin as used in the present study, on the other hand, has been shown not to alter food intake in rodents (38), but apparently allows access of insulin to brain areas regulating lipogenesis in WAT (Figure 10), indicating that our findings have uncovered a role for central insulin in the neuronal control of lipogenesis in addition to the well-documented adipocyte-autonomous inhibition of lipolysis. Taken together, our studies reveal differential, partially counterbalancing actions of insulin in the CNS, a catabolic function via control of food intake, and an anabolic function via indirect stimulation of lipogenesis. These data are in line with the notion that insulin acts as a primary hormone to control metabolism, while its overall energy homeostasis–regulating function appears to be minor compared with leptin.

Since adipokine secretion is tightly correlated with the amount of adipose tissue (reviewed in ref. 39), the differential regulation of WAT mass observed in $IR^{\Delta per}$ and $IR^{\Delta wb}$ mice implied consequences for circulating leptin and adiponectin levels. Leptin acts as an essential endocrine signal to the hypothalamus in the control of food intake and energy balance (40). Until today, the effects of insulin on leptin expression remain controversial. In vitro, while several studies could detect only mild or no effects of insulin on leptin expression (41–43), others have described a stimulating function for insulin on leptin expression and secretion in adipocytes (44–46). In vivo, the contradiction persists, as some groups report that insulin does not regulate leptin expression or secretion (47, 48), yet others have found that insulin increases plasma leptin levels (49, 50). After induction of peripheral insulin resistance, the $IR^{\Delta per}$ mice exhibited a dramatic increase in circulating leptin concentrations. In contrast, as previously published for transgenic models of lipodystrophy (51), $IR^{\Delta wb}$ mice displayed very low circulating leptin levels. However, when correlated with the amount of epigonadal fat, leptin levels were clearly increased to the same extent in $IR^{\Delta per}$ mice and in $IR^{\Delta wb}$ mice, as was the case

with plasma adiponectin levels. Thus, insulin appears to inhibit leptin secretion in a WAT-autonomic manner, consistent with the notion that loss of IR signaling specifically in adipocytes results in a rise in leptin secretion from the adipose tissue (9). In $IR^{\Delta wb}$ mice, although adipocyte-autonomous leptin secretion was increased, levels of circulating leptin were reduced as a consequence of the dramatic reduction in WAT mass. In $IR^{\Delta per}$ mice, however, the rise in serum leptin levels remained visible, due to the less dramatic reduction of WAT.

Concomitantly, adiponectin concentrations of $IR^{\Delta per}$ mice and $IR^{\Delta wb}$ mice were upregulated when correlated with WAT mass. This at first appears paradoxical, since it is well established that total plasma adiponectin is reduced in insulin-resistant subjects. However, other studies have previously reported a contradictory hyperadiponectinemia in patients with severe insulin resistance due to loss-of-function mutations in the IR (52). Strikingly, mutations in Akt2, a signaling molecule downstream of the IR in its signal transduction pathway, led to low leptin and adiponectin concentrations, indicating that elevated adiponectin concentrations in the presence of impaired IR function may reflect a loss of inhibition of adiponectin expression by an Akt2-independent insulin signaling pathway in adipocytes (52). Further studies have revealed that hyperadiponectinemia with loss of IR function is not dependent on developmental receptor dysfunction (53), a fact further supported by the inducible $IR^{\Delta per}$ and $IR^{\Delta wb}$ mouse models of insulin resistance employed here.

Leptin mediates its signaling-dependent effects by binding to the ObRb (54, 55). Both $IR^{\Delta wb}$ and $IR^{\Delta per}$ mice showed a surprising increase in mRNA expression of the ObRb in liver, as well as an increase in shedding of hepatic ObRb as binding protein (56). Upregulation of ObRb expression in liver could therefore be either a direct consequence of impaired insulin action in hepatocytes or other peripheral tissues, as it is observed to similar extents in both mouse models, or a secondary effect caused by increased leptin concentrations, as has been previously published (57). However, a similar increase in ObR expression in hepatocyte-specific IR knockout mice indicates that insulin suppresses ObR expression in liver in a cell-autonomous fashion (58).

Binding of leptin to the leptin receptor leads to receptor homodimerization, followed by activation of the JAKs, which in turn recruit and activate Stat proteins. Activated Stat proteins dimerize and translocate to the nucleus, where they bind to the DNA and activate transcription of target genes (reviewed in ref. 59). In addition to elevated leptin levels and increased ObRb mRNA and protein expression, $IR^{\Delta per}$ mice exhibit significantly increased phosphorylation of hepatic Stat3. In contrast, expression and tyrosine phosphorylation of Stat3 in $IR^{\Delta wb}$ mice that display low plasma leptin concentrations in the presence of elevated ObRb mRNA and protein expression are unaltered.

Also, *Il6* mRNA expression in the liver is significantly increased in $IR^{\Delta per}$ mice after induction of IR deficiency, whereas the expression remains unaltered in $IR^{\Delta wb}$ mice, indicating a role for central insulin action in the regulation of hepatic *Il6* mRNA. Since Stat3 is not only a target of leptin, but has recently been demonstrated as a target of the brain insulin signaling pathway by regulation of hepatic Il6 expression (24, 60), activation of hepatic Stat3 may be either a result of intact neuronal insulin signal transduction leading to an upregulation of hepatic *Il6* mRNA expression or a direct consequence of leptin signaling through the hepatic ObRb.

$IR^{\Delta wb}$ mice, lacking CNS insulin signaling, suffer from more severe hyperglycemia than $IR^{\Delta per}$ mice. Restoration of Stat3 tyrosine phosphorylation in $IR^{\Delta wb}$ mice results in a significant improvement of hyperglycemia to normal blood glucose levels. Although these experiments cannot ultimately rule out whether improved glucose metabolism in $IR^{\Delta per}$ mice versus $IR^{\Delta wb}$ mice is a consequence of Stat3 phosphorylation caused either by maintaining Il6 regulation, which is controlled by insulin signaling in the brain, or by elevated leptin concentrations in the presence of increased hepatic ObRb expression, these differential phenotypes of $IR^{\Delta per}$ and $IR^{\Delta wb}$ mice provide additional evidence for a physiologically relevant role of activated hepatic Stat3 signaling in glucose homeostasis in mice.

Pancreatic β cell IR knockout mice (βIRKO) suffer a loss of glucose-stimulated insulin secretion (13). A diminished first-phase insulin secretion is an early marker of β cell deterioration. The $IR^{\Delta per}$ mice, despite showing an IR deletion efficiency of more than 95% in pancreas (Figure 1C), did not exhibit a significant impairment in this pathway. Fasting plasma insulin levels in $IR^{\Delta wb}$ mice were significantly higher than those found in $IR^{\Delta per}$ mice, consistent with a more severe degree of insulin resistance in this mouse model due to higher blood glucose concentrations. Though significantly enlarged, no structural defects could be detected in pancreatic islets of $IR^{\Delta per}$ and $IR^{\Delta wb}$ mice, nor was the distribution of β cells altered in either mouse model. This is a clear indication that the IR is not required for acute β cell hyperproliferation, since β cell hyperplasia still occurs and the response to exogenously administered glucose is still detectable in $IR^{\Delta per}$ mice.

Taken together, our findings define CNS insulin action as a pivotal determinant of peripheral glucose and fat metabolism in the mouse. Our data underline the importance of hepatic Stat3 signaling in control of glucose metabolism and indicate what is to our knowledge a novel role for CNS insulin action in the regulation of adipocyte metabolism. Moreover, the differential phenotypes of mice with inducible versus constant gene inactivation reveals evidence for the occurrence of developmental changes in the latter type of models.

## Methods

*Animals*. Mice were housed in a specific pathogen–free facility at 22–24°C on a 12-h light/12-h dark cycle with the lights on at 6 am and were fed standard rodent chow (Teklad Global Rodent 2018; Harlan Winkelmann GmbH) containing 53.5% carbohydrates, 18.5% protein, and 5.5% fat. All animals had access to water ad libitum. Food was only withdrawn if required for an experiment. At the end of the study period, all animals were sacrificed by $CO_2$ anesthesia. All animal procedures and euthanasia were reviewed by the animal care committee of the University of Cologne, approved by local government authorities (Bezirksregierung Köln), and were in accordance with NIH guidelines.

*Generation of mice*. $IR^{flox/flox}$ mice were bred with mice heterozygous for the expression of a fusion protein consisting of a mutated ligand binding domain of the ER and the Cre recombinase from the Rosa26 locus ($Rosa26CreER^{T2}$) (18). Resulting offspring were further intercrossed with $IR^{flox/flox}$ mice to yield $IR^{flox/flox}Rosa26CreER^{T2+/-}$ mice. Tamoxifen-treated $IR^{flox/flox}Rosa26CreER^{T2}$–positive mice are referred to as $IR^{\Delta per}$ mice, and tamoxifen-treated $IR^{flox/flox}Rosa26CreER^{T2}$–negative mice were used as respective controls ($Control^{\Delta per}$). Genotyping was performed by PCR on DNA extracted from tail biopsies using customized primers: sense, 5′-GATGTGCACCCCATGTCTG-3′, antisense, 5′-CTGAATAGCTGAGACCACAG-3′ (IR allele); and sense, 5′-ACCTGAAGATGTTCGCGATTATCT-3′, antisense, 5′-ACCGTCAGTACGTGAGATATCTT-3′ ($CreER^{T2}$ transgene).

Mice expressing a shRNA against the IR were generated as previously described (20). Doxycycline-treated shRNA are referred to as $IR^{\Delta wb}$ mice, and doxycycline-treated wild-type littermates as $Control^{\Delta wb}$ mice.

*Experimental setup*. On 5 consecutive days at the age of 10–12 weeks, 5 mg tamoxifen was administered to $IR^{\Delta per}$ and $Control^{\Delta per}$ mice by oral gavage using a 22-gauge feeding needle. Ten- to 12-week-old shRNA-expressing mice ($IR^{\Delta wb}$) and C57BL/6 littermates ($Control^{\Delta wb}$) were administered drinking water supplemented with 10% sucrose (AppliChem GmbH) plus 2 mg/ml Doxycycline Hyclate (D-9891; Sigma-Aldrich) to induce the H1/U6 promoter over a period of 30 days. Doxycycline-supplemented water was changed every 2 days. Body weight and blood glucose levels were monitored daily. Food intake was measured over a period of 30 days, and daily food intake was calculated as the average intake of chow over the time stated.

*Analytical procedures*. Blood glucose values were determined from whole venous blood using an automatic glucose monitor (GlucoMen GlycÓ; A. Menarini Diagnostics). Insulin, leptin, and adiponectin levels in serum were measured by ELISA using mouse standards according to the manufacturer's guidelines (Mouse/Rat Insulin ELISA; Crystal Chem Inc.; ACTIVE Murine Leptin ELISA; Diagnostics Systems Laboratories Inc.; Quantikine Mouse Adiponectin/Acrp30 ELISA; R&D Systems). Free fatty acids were measured using the Nefa C Kit (Wako Chemicals) according to the manufacturer's protocols. Triglycerides were measured from serum using a clinical diagnostic system (Hitachi).

*Glucose tolerance test*. Glucose tolerance tests were performed on animals that had been fasted overnight for 16 hours. Animals were injected with 2 g/kg body weight of glucose into the peritoneal cavity. Glucose levels were determined in blood collected from the tail tip immediately before and 15, 30, 60, and 120 minutes after the injection.

*Glucose-stimulated insulin secretion*. All animals were fasted overnight for 16 hours. Blood samples were collected from mice prior to an intravenous injection of 2 g/kg body weight of glucose. Further blood samples were amassed 2, 5, 15, 30, and 60 minutes after the injection, and serum insulin levels were determined.

*Leptin restoration*. Sixteen days after start of administration of doxycycline-supplemented water, 5 $IR^{\Delta wb}$ mice and 5 respective controls were anesthetized by intraperitoneal avertin injection and subcutaneously implanted with Alzet mini-osmotic pumps (model 2001; Charles River Laboratories), which secrete 0.5 μg leptin/μl/h over a period of 7 days. Food intake, body weight, and blood glucose were measured daily over the entire period of the experiment, starting 2 days prior to pump implant. Serum samples were taken every 2 days to monitor circulating leptin concentrations. Seven days after pump implant, mice were sacrificed and hepatic Stat3 phosphorylation was assessed by western blot analysis.

*Nuclear magnetic resonance*. Thirty days after start of either tamoxifen or doxycycline administration, whole body composition of live animals was determined using the NMR Analyzer Minispec mq7.5 (Bruker Optik).

*Insulin signaling*. Mice were anesthetized by intraperitoneal injection of avertin (tribromoethyl alcohol and *tert*-amyl alcohol; Sigma-Aldrich), and adequacy of the anesthesia was ensured by loss of pedal reflexes. The abdominal cavity of the mice was opened, and 125-μl samples containing 5 U regular human insulin (Actrapid; Novo Nordisk) diluted in 0.9% saline were injected into the vena cava inferior. Sham injections were performed with 125 μl of 0.9% saline. Samples of liver and skeletal muscle were harvested 2 and 5 minutes after injection, respectively, and proteins were extracted from tissues for western blot analysis.

*Intracerebroventricular insulin infusion*. For intracerebroventricular cannula implantation, 11-week-old male C57BL/6 mice were anesthetized as previously described and placed in a stereotactic device (Stoelting; Foehr Medical Instruments GmbH). A sterile osmotic pump connector cannula (Alzet Brain Infusion Kit 3; Charles River Laboratories) was implanted into the left lateral brain ventricle (–0.2 mm anterior and 1.0 mm lateral relative to bregma and 2.3 mm below skull surface). The pedestal of the cannula was attached to the skull with cyanoacrylate adhesive. The cannula was connected to an Alzet mini-osmotic pump (model 1002; Charles River Laboratories) with a secretion rate of 200 μU insulin/d over a period of 7 days. After 7 days, animals were sacrificed and correct positioning of the intracerebroventricular cannula was verified in each animal by injection of 1% methylen blue. WAT mass was removed, weighed, and processed for histological analysis, and RNA was extracted using the Qiagen RNeasy Kit according to the manufacturer's guidelines.

*Western blot analysis*. Indicated tissues were dissected and homogenized in lysis buffer (50 mM HEPES, pH 7.4, 1% Triton X-100, 0.1 M sodium fluoride, 10 mM EDTA, 50 mM sodium chloride, 10 mM sodium orthovanadate, 0.1% SDS, 10 μg/ml aprotinin, 2 mM benzamidine, and 2 mM PMSF) using a Polytron homogenizer (IKA Werke). Particulate matter was removed by centrifugation at 10,000 *g* for 1 h at 4°C. Western blot analyses were performed according to standard protocols using antibodies against the IR β subunit (Santa Cruz Biotechnology Inc.), ObRb (Santa Cruz Biotechnology Inc.), Stat3, pStat3 (Santa Cruz Biotechnology Inc.) and pAKT (Cell Signaling Technology Inc.), with antibodies raised against AKT (Cell Signaling Technology Inc.) as loading control.

*Densitometrical analysis*. Protein expression was assessed by western blot analysis, and bands were measured in intensity per $mm^2$ using Quantity One Software (Bio-Rad). After background subtraction, each sample was normalized to an internal loading control (Akt). Average protein expression of control mice was set to 100% and compared with protein expression of knockout animals.

*Southern blot analysis*. Genomic DNA was extracted from indicated tissues as previously described. Phenol chloroform–extracted DNA (10 μg) was digested overnight using NcoI restriction enzyme (MBI Fermentas GmbH) and separated on a 0.8% agarose gel. The DNA was subsequently transferred and immobilized on a nylon membrane (Amersham). A probe was amplified using 2 customized primers, 5′-CCATGGGTCCATAAGCTATC-3′ (sense) and 5′-AGTGATGAGATGGCTCATTAG-3′ (antisense), and labeled with $^{32}P$ using the Ladderman DNA Labeling Kit (TaKaRa; Cambrex Bio Science). Hybridization of the probe to its corresponding sequence of the murine *IR* gene on the nylon membrane was performed overnight at 68°C. Unspecifically bound probe was washed off with 1% SSC, 0.1% SDS (AppliChem GmbH) at 68°C for 20 minutes.

*Tissue preparation for immunohistochemistry*. Pancreatic tissue was excised and snap-frozen in Jung Tissue Freezing Medium (Leica Microsystems Nussloch GmbH), transferred to a cryostat (CM3050S; Leica Microsystems Nussloch GmbH), and cut into 7-μm-thin sections. Specimens were collected on clean poly-L-lysine–coated glass slides (Polysine; Menzel GmbH & Co.), dried at room temperature overnight, and then stained using H&E for general histology. WAT was dissected, fixed overnight in 7% formaldehyde, and then embedded for paraffin sections. Subsequently, 7-μm-thick sections were deparaffinized and stained with H&E for general histology. H&E (Sigma-Aldrich) staining was performed according to standard protocols. Pancreatic tissues were also stained for insulin (DakoCytomation) and glucagon (DakoCytomation) using a 1:20 and 1:75 dilution, respectively. Slides had been previously fixed in acetone at 4°C for 10 minutes and air dried. Both stainings were incubated with a secondary antibody consisting of a 1:100 dilution of horseradish peroxidase–coupled anti-rabbit IgG (Vector Laboratories/Linaris GmbH). Tissues were counterstained 2 minutes with Mayers hematoxylin, then washed in tepid water for 5 minutes. Stainings were analyzed with an Axioskop 40 microscope (Carl Zeiss MicroImaging GmbH), and β cell mass and adipocyte

size was determined using the microscopy software AxioVision (Carl Zeiss MicroImaging GmbH).

*mRNA expression*. Hepatic mRNA levels were measured by quantitative RT-PCR on RNA extracted from dissected liver tissue. Total RNA for each liver was quantified by spectrophotometry after purification using the Qiagen RNeasy Kit (Qiagen). We reverse-transcribed 200 ng of each total RNA sample according to the manufacturer's protocols (Eurogentec), then PCR-amplified each sample using TaqMan Principles ABI Prism 7700 Sequence Detection System (Applied Biosystems). Relative expression of *ObRb*, *G6P*, and *Il6* mRNA was determined using standard curves based on hepatic cDNA, and *lipoprotein lipase* mRNA was determined using standard curves based on cDNA derived from WAT. Samples were adjusted for total RNA content by glucuronidase and Hprt-1 RNA quantitative PCR. Calculations were performed by a comparative method ($2^{-\Delta\Delta CT}$).

*Statistics*. All data sets were analyzed for statistical significance using a 2-tailed unpaired Student's *t* test. All *P* values below 0.05 were considered significant. Data sets of experiments displayed in Figures 3C and 4A were analyzed in addition by ANOVA using SPSS 16.0 software. All ANOVA values below 0.05 were considered significant.

## Acknowledgments

The authors thank Gisela Schmall for excellent secretarial assistance, Jens Alber and Julia Baumgartl for outstanding technical assistance, and Andrew L. Croxford for critical reading of the manuscript. This work was supported by grants from the Center for Molecular Medicine Cologne (TV2) and the European Union (LSHM-CT-2003-503041, to J.C. Brüning), the Fritz Thyssen Stiftung (Az. 10.04.1.153/Az. 10.06.2.175, to J.C. Brüning), the European Foundation for the Study of Diabetes/Lilly European Diabetes Research Programme (to J.C. Brüning), and the DFG (Br. 1492/7-1, to J.C. Brüning).

Received for publication November 27, 2006, and accepted in revised form February 27, 2008.

Address correspondence to: Jens C. Brüning, Institute for Genetics, Department of Mouse Genetics and Metabolism, Zülpicher Strasse 47, 50674 Köln, Germany. Phone: 49-221-470-2467; Fax: 49-221-470-5185; E-mail: jens.bruening@uni-koeln.de.

1. Lillioja, S., et al. 1993. Insulin resistance and insulin secretory dysfunction as precursors of non-insulin-dependent diabetes mellitus. Prospective studies of Pima Indians. *N. Engl. J. Med.* **329**:1988–1992.
2. Martin, B.C., et al. 1992. Role of glucose and insulin resistance in development of type 2 diabetes mellitus: results of a 25-year follow-up study. *Lancet.* **340**:925–929.
3. Saltiel, A.R., and Kahn, C.R. 2001. Insulin signalling and the regulation of glucose and lipid metabolism. *Nature.* **414**:799–806.
4. Nigro, J., Osman, N., Dart, A.M., and Little, P.J. 2006. Insulin resistance and atherosclerosis. *Endocr. Rev.* **27**:242–259.
5. Plum, L., Belgardt, B.F., and Bruning, J.C. 2006. Central insulin action in energy and glucose homeostasis. *J. Clin. Invest.* **116**:1761–1766.
6. Semenkovich, C.F. 2006. Insulin resistance and atherosclerosis. *J. Clin. Invest.* **116**:1813–1822.
7. Accili, D., et al. 1996. Early neonatal death in mice homozygous for a null allele of the insulin receptor gene. *Nat. Genet.* **12**:106–109.
8. Joshi, R.L., et al. 1996. Targeted disruption of the insulin receptor gene in the mouse results in neonatal lethality. *EMBO J.* **15**:1542–1547.
9. Bluher, M., et al. 2002. Adipose tissue selective insulin receptor knockout protects against obesity and obesity-related glucose intolerance. *Dev. Cell.* **3**:25–38.
10. Bruning, J.C., et al. 2000. Role of brain insulin receptor in control of body weight and reproduction. *Science.* **289**:2122–2125.
11. Bruning, J.C., et al. 1998. A muscle-specific insulin receptor knockout exhibits features of the metabolic syndrome of NIDDM without altering glucose tolerance. *Mol. Cell.* **2**:559–569.
12. Fisher, S.J., and Kahn, C.R. 2003. Insulin signaling is required for insulin's direct and indirect action on hepatic glucose production. *J. Clin. Invest.* **111**:463–468.
13. Kulkarni, R.N., et al. 1999. Tissue-specific knockout of the insulin receptor in pancreatic beta cells creates an insulin secretory defect similar to that in type 2 diabetes. *Cell.* **96**:329–339.
14. Baumgartl, J., et al. 2006. Myeloid lineage cell-restricted insulin resistance protects apolipoproteinE-deficient mice against atherosclerosis. *Cell Metab.* **3**:247–256.
15. Vicent, D., et al. 2003. The role of endothelial insulin signaling in the regulation of vascular tone and insulin resistance. *J. Clin. Invest.* **111**:1373–1380.
16. Kuhbandner, S., et al. 2000. Temporally controlled somatic mutagenesis in smooth muscle. *Genesis.* **28**:15–22.
17. Sohal, D.S., et al. 2001. Temporally regulated and tissue-specific gene manipulations in the adult and embryonic heart using a tamoxifen-inducible Cre protein. *Circ. Res.* **89**:20–25.
18. Seibler, J., et al. 2003. Rapid generation of inducible mouse mutants. *Nucleic Acids Res.* **31**:e12.
19. Seibler, J., et al. 2005. Single copy shRNA configuration for ubiquitous gene knockdown in mice. *Nucleic Acids Res.* **33**:e67.
20. Seibler, J., et al. 2007. Reversible gene knockdown in mice using a tight, inducible shRNA expression system. *Nucleic Acids Res.* **35**:e54.
21. Fain, J.N., Kovacev, V.P., and Scow, R.O. 1966. Antilipolytic effect of insulin in isolated fat cells of the rat. *Endocrinology.* **78**:773–778.
22. Kovacev, V.P., and Scow, R.O. 1966. Effect of hormones on fatty acid release by rat adipose tissue in vivo. *Am. J. Physiol.* **210**:1199–1208.
23. Lavis, V.R., and Williams, R.H. 1973. Lipolytic effects of high concentrations of insulin on isolated fat cells. Enhancement of the response to lipolytic hormones. *Diabetes.* **22**:629–636.
24. Inoue, H., et al. 2006. Role of hepatic STAT3 in brain-insulin action on hepatic glucose production. *Cell Metab.* **3**:267–275.
25. Konner, A.C., et al. 2007. Insulin action in AgRP-expressing neurons is required for suppression of hepatic glucose production. *Cell Metab.* **5**:438–449.
26. Obici, S., Feng, Z., Karkanias, G., Baskin, D.G., and Rossetti, L. 2002. Decreasing hypothalamic insulin receptors causes hyperphagia and insulin resistance in rats. *Nat. Neurosci.* **5**:566–572.
27. Rahmouni, K., et al. 2004. Hypothalamic PI3K and MAPK differentially mediate regional sympathetic activation to insulin. *J. Clin. Invest.* **114**:652–658.
28. Strubbe, J.H., and Mein, C.G. 1977. Increased feeding in response to bilateral injection of insulin antibodies in the VMH. *Physiol. Behav.* **19**:309–313.
29. Buettner, C., et al. 2005. Severe impairment in liver insulin signaling fails to alter hepatic insulin action in conscious mice. *J. Clin. Invest.* **115**:1306–1313.
30. Gelling, R.W., et al. 2006. Insulin action in the brain contributes to glucose lowering during insulin treatment of diabetes. *Cell Metab.* **3**:67–73.
31. Obici, S., Zhang, B.B., Karkanias, G., and Rossetti, L. 2002. Hypothalamic insulin signaling is required for inhibition of glucose production. *Nat. Med.* **8**:1376–1382.
32. Okamoto, H., Obici, S., Accili, D., and Rossetti, L. 2005. Restoration of liver insulin signaling in Insr knockout mice fails to normalize hepatic insulin action. *J. Clin. Invest.* **115**:1314–1322.
33. Plum, L., et al. 2006. Enhanced PIP3 signaling in POMC neurons causes KATP channel activation and leads to diet-sensitive obesity. *J. Clin. Invest.* **116**:1886–1901.
34. Edgerton, D.S., et al. 2006. Insulin's direct effects on the liver dominate the control of hepatic glucose production. *J. Clin. Invest.* **116**:521–527.
35. Cherrington, A.D. 2005. The role of hepatic insulin receptors in the regulation of glucose production. *J. Clin. Invest.* **115**:1136–1139.
36. Theander-Carrillo, C., et al. 2006. Ghrelin action in the brain controls adipocyte metabolism. *J. Clin. Invest.* **116**:1983–1993.
37. Grillo, C.A., et al. 2007. Lentivirus-mediated downregulation of hypothalamic insulin receptor expression. *Physiol. Behav.* **92**:691–701.
38. Manin, M., Balage, M., Larue-Achagiotis, C., and Grizard, J. 1988. Chronic intracerebroventricular infusion of insulin failed to alter brain insulin-binding sites, food intake, and body weight. *J. Neurochem.* **51**:1689–1695.
39. Coll, A.P., Farooqi, I.S., and O'Rahilly, S. 2007. The hormonal control of food intake. *Cell.* **129**:251–262.
40. Zhang, Y., et al. 1994. Positional cloning of the mouse obese gene and its human homologue. *Nature.* **372**:425–432.
41. Slieker, L.J., et al. 1996. Regulation of expression of ob mRNA and protein by glucocorticoids and cAMP. *J. Biol. Chem.* **271**:5301–5304.
42. Murakami, T., Iida, M., and Shima, K. 1995. Dexamethasone regulates obese expression in isolated rat adipocytes. *Biochem. Biophys. Res. Commun.* **214**:1260–1267.
43. MacDougald, O.A., Hwang, C.S., Fan, H., and Lane, M.D. 1995. Regulated expression of the obese gene product (leptin) in white adipose tissue and 3T3-L1 adipocytes. *Proc. Natl. Acad. Sci. U. S. A.* **92**:9034–9037.
44. Gettys, T.W., Harkness, P.J., and Watson, P.M. 1996. The beta 3-adrenergic receptor inhibits insulin-stimulated leptin secretion from isolated rat adipocytes. *Endocrinology.* **137**:4054–4057.
45. Bradley, R.L., and Cheatham, B. 1999. Regulation of ob gene expression and leptin secretion by insulin and dexamethasone in rat adipocytes. *Diabetes.* **48**:272–278.
46. Barr, V.A., Malide, D., Zarnowski, M.J., Taylor, S.I., and Cushman, S.W. 1997. Insulin stimulates both leptin secretion and production by rat white adipose tissue. *Endocrinology.* **138**:4463–4472.
47. Vidal, H., et al. 1996. The expression of ob gene

is not acutely regulated by insulin and fasting in human abdominal subcutaneous adipose tissue. *J. Clin. Invest.* **98**:251–255.
48. Dagogo-Jack, S., Fanelli, C., Paramore, D., Brothers, J., and Landt, M. 1996. Plasma leptin and insulin relationships in obese and nonobese humans. *Diabetes.* **45**:695–698.
49. Malmstrom, R., Taskinen, M.R., Karonen, S.L., and Yki-Jarvinen, H. 1996. Insulin increases plasma leptin concentrations in normal subjects and patients with NIDDM. *Diabetologia.* **39**:993–996.
50. Kolaczynski, J.W., et al. 1996. Acute and chronic effects of insulin on leptin production in humans: Studies in vivo and in vitro. *Diabetes.* **45**:699–701.
51. Shimomura, I., et al. 1998. Insulin resistance and diabetes mellitus in transgenic mice expressing nuclear SREBP-1c in adipose tissue: model for congenital generalized lipodystrophy. *Genes Dev.* **12**:3182–3194.
52. Semple, R.K., et al. 2006. Elevated plasma adiponectin in humans with genetically defective insulin receptors. *J. Clin. Endocrinol. Metab.* **91**:3219–3223.
53. Semple, R.K., et al. 2007. Paradoxical elevation of high-molecular weight adiponectin in acquired extreme insulin resistance due to insulin receptor antibodies. *Diabetes.* **56**:1712–1717.
54. Tartaglia, L.A., et al. 1995. Identification and expression cloning of a leptin receptor, OB-R. *Cell.* **83**:1263–1271.
55. Baumann, H., et al. 1996. The full-length leptin receptor has signaling capabilities of interleukin 6-type cytokine receptors. *Proc. Natl. Acad. Sci. U. S. A.* **93**:8374–8378.
56. Ge, H., Huang, L., Pourbahrami, T., and Li, C. 2002. Generation of soluble leptin receptor by ectodomain shedding of membrane-spanning receptors in vitro and in vivo. *J. Biol. Chem.* **277**:45898–45903.
57. Cohen, P., et al. 2005. Induction of leptin receptor expression in the liver by leptin and food deprivation. *J. Biol. Chem.* **280**:10034–10039.
58. Cohen, S.E., et al. 2007. High circulating leptin receptors with normal leptin sensitivity in liver-specific insulin receptor knock-out (LIRKO) mice. *J. Biol. Chem.* **282**:23672–23678.
59. Margetic, S., Gazzola, C., Pegg, G.G., and Hill, R.A. 2002. Leptin: a review of its peripheral actions and interactions. *Int. J. Obes. Relat. Metab. Disord.* **26**:1407–1433.
60. Inoue, H., et al. 2004. Role of STAT-3 in regulation of hepatic gluconeogenic genes and carbohydrate metabolism in vivo. *Nat. Med.* **10**:168–174.